GD/C-DBE-66-003
Space Science Laboratory

PREDICTION OF TOTAL EMISSIVITY OF NITROGEN-BROADENED AND SELF-BROADENED HOT WATER VAPOR

by

C. B. Ludwig
and
C. C. Ferriso

FEBRUARY 1966

Technical Report

Research and Advanced Technology Department

CONTRACT NAS 8-11363

GENERAL DYNAMICS CONVAIR

GD/C-DBE-66-003
Space Science Laboratory

PREDICTION OF TOTAL EMISSIVITY OF NITROGEN-BROADENED AND SELF-BROADENED HOT WATER VAPOR

by

C. B. Ludwig
and
C. C. Ferriso

FEBRUARY 1966

This work was sponsored in part by The George C. Marshall Space Flight Center of the National Aeronautics and Space Administration under Contract NAS 8-11363. The work was administered under the direction of the Aero-Astrodynamics Laboratory (R-AERO-R) of The George C. Marshall Space Flight Center of Huntsville, Alabama. This work was also sponsored in part by General Dynamics/Convair Research Funds.

GENERAL DYNAMICS CONVAIR

N66-38114

ABSTRACT

Predictions of the total emissivity of nitrogen-broadened and self-broadened water vapor in the temperature range from 600° to 3000°K and optical depths from 0.1 to 10,000 cm atm are made, based on a set of spectral absorption coefficients, fine structure parameters which are temperature dependent but frequency-independent, and the assumption that the curve of growth is given by a statistical band model. The uncertainties in the predicted values are calculated on the basis of the uncertainties in the absorption coefficients and the fine structure parameters at various temperatures. A comparison of these predictions with available limited experimental results shows satisfactory agreement for the total emissivities and the individual band emissivities of water vapor.

Author

INTRODUCTION

In a previous report,[1] we have calculated the upper limit (high-pressure limit) to the total emissivity of hot water vapor as a function of optical pathlengths and temperatures. In this limit the spectrum is smeared out. The fine structure parameter representing the spectrum is set to infinity (i.e., the line spacing is equal to zero) and the gas follows Beer's law approaching blackbody emission with increasing optical depth.

In real gases, the fine structure parameter is not infinite and the blackbody emission is approached more slowly than in Beer's law with increasing optical depth. The functional relationship between the emissivity and optical depth is called the "curve of growth." A number of theoretical models for the curves of growth have been developed.[2,3] Goody[3] has treated the absorptivity of gas whose spectral lines are distributed statistically both in position and intensity and showed the applicability to water vapor. The expression for the curve of growth contains the mean spectral absorption coefficient, the optical depth, and a rotational fine structure term which is dependent on a collision parameter and the mean line spacing. Moreover, both the absorption coefficient, as well as the fine structure term, are functions of the temperature and frequency. At present, these functions are known only in limited spectral regions and temperature ranges. It was shown[4] that a set of mean spectral absorption coefficients could be derived by band-averaging the fine structure term and adjusting it in such a way that the integral of the absorption coefficients over a given vibration-rotation band

results in the known value of the band intensity.

It is the purpose of the present work to use a set of spectral absorption coefficients and the temperature dependent but frequency independent fine structure term to predict the total emissivity of water vapor between 600° and 3000°K, as a function of the optical path in the range from 0.1 to 10,000 cm atm. Although the spectral mean absorption coefficients are based on experimental measurements up to 2750°K, the fine structure term is known only to 1800°K. In addition, the statistical band model by Goody has been shown to be valid for very long paths at room temperature only.[5] Therefore, the predictions of the total emissivities for high temperatures and long paths are not verified as yet. Nevertheless, we believe our predictions will be useful as first approximations since the results compare favorably with other experimental results.

We have made comparisons of our predictions with existing experimental results, both for the total emissivities as well as the band emissivities. The first comparison is made with Hottel's standard charts.[6] It turns out that wherever Hottel's data are based on actual experimental data, the agreement is good, but that in regions where Hottel's data are extrapolations, disagreement exists. For the second comparison, the collected band emissivities by Edwards and coworkers,[7] Burch and Gryvnak,[8] and by the present authors were used. The agreement is found to be satisfactory.

CALCULATIONAL PROCEDURE

The total emissivity of a gas, ϵ_T, is given by

$$\epsilon_T(T, p_T, c, \ell) = \frac{1}{\sigma T^4} \int_0^\infty \epsilon(\omega, T)\, N^\circ(\omega, T)\, d\omega \qquad (1)$$

where $N^{o}(\omega,T)$ is the blackbody energy, $\epsilon(\omega,T)$ is the spectral gas emissivity, p_T the total pressure, c the concentration of the emitting species, ℓ the geometric pathlength of the radiating gas, σ is the Stefan Boltzmann constant, T the temperature in °K, and ω the wavenumber.

In the statistical model, the spectral emissivity is given by

$$\epsilon(\omega) = 1-\exp\left[-\frac{W(\omega)}{d(\omega)}\right] \tag{2}$$

where $W(\omega)$ is the average equivalent width and $d(\omega)$ is the average line spacing. Goody has shown[3] that the curves of growth are quite insensitive to the choice of the line intensity distribution functions. When the smoothed absorption coefficient and mean line width to line spacing ratio are chosen so that the curves of growth agree in the optically thin and in the square root limits, the values of $(\frac{W}{d})$ corresponding to a delta function, an exponential or a 1/S distribution differ by at most 25%.

In the present analysis, we have used the intermediate form corresponding to an exponential distribution of line intensities:

$$\frac{W}{d} = \frac{k(\omega)u}{\sqrt{1+\frac{k(\omega)u}{4\bar{a}}}} \tag{3}$$

where $k(\omega)$ is the mean absorption coefficient, u the optical depth (at STP), and $\bar{a}$ is the band averaged fine structure parameter. In several cases a 1/S distribution of line intensities[9] was used in the form $\frac{W(\omega)}{d(\omega)} = 2a\left(\sqrt{1+\frac{k(\omega)u}{a}}-1\right)$ and compared to the present analysis. The differences in $\bar{a}$ are found to be less than 40%. The parameter $\bar{a}$ is

proportional to the band averaged value of the ratio of the collision half-width to the line spacing, γ/d. The collision half-width can be written as

$$\gamma = \gamma^{o}\, p_T \sqrt{\frac{T_o}{T}} \left[c\left(\sqrt{\frac{T_o}{T}} + \sigma' \right) + (1-c)\sigma_x \right] \tag{4}$$

where γ^{o} is the half-width due to water-water collisions at T_o and 1 atm, c is the mole fraction of water, σ' is the ratio of the broadening ability of the non-resonant H_2O dipoles to the self-broadening ability of H_2O, and σ_x is the ratio of the broadening ability of the nonabsorbing gas to the self-broadening ability of H_2O. Equation (4) can be rewritten in terms of an equivalent pressure, p_e

$$\gamma = \gamma^{o}\, \sigma_x \sqrt{\frac{T_o}{T}}\, p_e \quad . \tag{5}$$

where

$$p_e = p_T \left[c\left(\frac{1}{\sigma_x} \sqrt{\frac{T_o}{T}} + \frac{\sigma'}{\sigma_x} - 1 \right) + 1 \right] . \tag{6}$$

Note, that at $T = T_o$ and $\sigma' = 0$, Eq. (6) reduces to

$$p_e = \left[p_T + \left(\frac{1}{\sigma_x} - 1 \right) p_{H_2O} \right] \tag{6a}$$

which is identical to an expression frequently used in the literature,[10] since $1/\sigma_x = B$.

The average line spacings $\bar{d}(T)$ were obtained from 80 spectra of the 2.7- and 6.3-μ bands. Each point has about a factor of 2 uncertainty. The overall spread of points is mostly within a factor of 5, but can be

as large as a factor of 10 (at 1200°K for instance). The straight line is a least square fit to the points and is given by

$$\bar{d}(T) = \exp[-.00106T + 1.21] \qquad (7)$$

One point at 2200°K is obtained from the rotational band. The majority of points is restricted to temperatures < 1800°K.

The two combination bands at 1.87 μ and 1.38 μ are much weaker than the fundamental bands. Room temperature absorption spectra of the 1.87-μ band indicate that the value of $\bar{d}$ is practically the same as that obtained from the two fundamental bands. Values of $\bar{d}$ derived from the data presented by Nelson[11] are generally higher than values of $\bar{d}$ obtained from his data for the two fundamental bands, but the experimental uncertainty in his measurements does not permit any definite conclusions. In the absence of further information, it is assumed that the $\bar{d}(T)$ for the two combination bands is the same as that deduced for the fundamental bands. The average absorption coefficients were given in Ref. 4. In general, the mean deviation of the absorption coefficients taken from the individual spectra is within ± 20%. In some portions of the spectra, where the absorption coefficient changes rapidly, a much greater spread in the individual absorption coefficients was observed. The large spread here is probably introduced by small errors in the wavenumber calibration of the different measuring instruments.

RESULTS

The calculation was performed for seven temperatures, five total pressures, and three partial pressures. Nitrogen was chosen as the

foreign-gas broadener.† The following parameters were used in the calculation: $\gamma^{o} = 0.5$ cm^{-1}atm^{-1}; $\sigma_x = 0.165$; $\sigma' = 0.1$; T = 300°, 600°, 1000°, 1500°, 2000°, 2500°, and 3000°K; c = 0, 0.5, and 1.0; p_T = 0.1, 0.5, 1.0, 2.0, and 5.0 atm. The results of the calculations are given in Figs. 1-15, where the ϵ_T is plotted versus $p\ell$ (cm atm) at the different temperatures. Each graph is for one condition of c and p_T. In order to show the difference between this calculation and the total emissivity calculation in the high pressure limit, we have plotted the ratio $\eta(p_e,T) = (\epsilon_T/\epsilon_T')$ as a function of the equivalent pressure p_e, where ϵ_T' is the total emissivity in the high pressure limit. Figure 16 is a plot of ϵ_T' versus $p\ell$, and Figs. 17-22 are plots of η versus p_e for different temperatures. The smaller the value of η, the greater is the influence of the fine structure parameter. For large values of equivalent pressure, the ratio η approaches unity, i.e., the high pressure limit. It is noted that the greatest influence is for optical depths between 10 to 100 cm atm.

ERROR ANALYSIS

The error analysis is based on the uncertainties in the spectral absorption coefficient k, the line spacing d, the foreign-gas broadener effect σ_x, and the interaction of non-resonating dipoles σ'. Based on the analysis in Ref. 4, we have chosen $\Delta k = \pm 20\%$ and $\Delta d = \pm 100\%$. In addition, we have set $\Delta\sigma_x = \pm 20\%$ and $\Delta\sigma' = \pm 100\%$. The results are shown in Figs. 23-25, as a function of pL for the three temperatures, 555°, 1670°, and 2780°K. In Fig. 26, we show the error as a function of the

---

†In a subsequent report we will discuss the influence of other foreign-gas broadeners.

temperatures for three selected optical depths. Although the uncertainties selected for the individual parameters were quite large, the total emissivities are affected by less than ± 22% for pL ≥ 1000 cm atm. It is to be noted that the error decreases with increasing optical depths. At optical depths greater than 1000 cm atm, the influence of additional uncertainty on any of the four parameters will be small.

An additional study of the influence of the S^{-1} model[9] on the total emissivity was made. It turns out that ϵ_T becomes larger when the S^{-1} line intensity distribution is used instead of the exponential one. In Fig. 27, the deviation is plotted versus pL for the three temperatures, 555°, 1670°, and 2780°K.

COMPARISON WITH EXPERIMENTAL DATA

The first comparison (a) was made with the total emissivity tables given by Hottel and Egbert[6] where c = 0 and p_T = 1 atm, including the correction chart for different partial and total pressures. The second comparison (b) was made with existing experimental band emissivities.

a) Comparison with Hottel and Egbert

We have calculated ϵ_T at T = 555°K (1000°R), 1670°K (3000°R) between 0.1 cm atm (0.003 ft-atm) and 10,000 cm atm (300 ft-atm) with zero partial pressure at 1 atm total pressure and nitrogen broadening (σ_x = 0.165). The result of the calculation together with Hottel's[6] values is shown in Fig. 28. Hottel's extrapolated values are the dashed lines. It is found that satisfactory agreement exists between our calculation and Hottel's data in most regions. Only at the higher temperatures and greater optical depths (Hottel's extrapolated regions) do we find greater discrepancies.

In order to correct for the effect of total and partial pressure on the total emissivity, Hottel and Egbert[6] gave a chart of the ratio ϵ/ϵ^* versus $0.5\ (p_T + p_{H_2O})$, where ϵ is the total emissivity of water vapor, ϵ^* is the total emissivity of water vapor at 1 atm total pressure and zero partial pressure of H_2O. In this chart, curves are given for optical depths between 0.05 ft-atm and 10 ft-atm. To compare our results with the correction chart, we have calculated the ratios ϵ/ϵ^* for $.1 \leq p_T \leq 5.0$ atm, $c = 0$, 0.5, and 1.0, and $600 \leq T \leq 3000°K$ at $pL = 1$ cm atm and $pL = 100$ cm atm, which are approximately the limits Hottel has used. The comparison for $pL \sim 1$ cm atm is shown in Fig. 29. The vertical bars represent the range, in which the ratio ϵ/ϵ^* varies for different concentrations and temperatures. The values at the highest temperature (3000°K) are always at that end of the bars which is closest to $\epsilon/\epsilon^* = 1$. This behavior is to be expected, since for small optical depths the ratio ϵ/ϵ^* should approach unity, and first at higher temperatures. The agreement between our data and Hottel's curve is poor at this optical depth. It must be remembered that Hottel's curve (at $pL = 1.5$ cm atm) is based on only a few measurements of several investigators, whose data show considerable spread. The comparison at $pL = 300$ cm atm is shown in Fig. 30. In this case, the agreement is very good. The variation of the ratio ϵ/ϵ^* with temperature is less than in the case of $pL = 1$ cm atm, a fact which is apparent also in Hottel and Egbert's original plots (see Fig. 15 of Ref. 6). These authors chose not to show this temperature variation in order to simplify their final working curves.

b) Comparison with Band Emissivities

Over the years many measurements of the band emissivities up to

1200°K were made by different workers. Recently, Edwards, et al,[7] have summarized these measurements and presented correlations in terms of wide-band adaptation of the Mayer-Goody statistical band model using a mean line width to line spacing ratio and spectral band contours calculated in the just-overlapping line model by Gray.[12] They then compared the measured band absorptances with their calculated values and gave the RMS value of the deviations for each individual band. We performed a similar comparison and the results are given in Table I. The first entries for each band were taken from Edwards, et al,[7] including the entries up to the temperature of 1111°K. The next entries in the 2.7-μ band (900°-1500°K) were taken from Burch and Gryvnak,[8] while the rest of the data were taken from our own measurements. At the end of the listing for each band, the RMS value of the deviations is given. Except for the rotational band, the RMS values are within ± 21%.

SUMMARY

Total emissivities of nitrogen-broadened and self-broadened water vapor are predicted in the temperature range from 600°K to 3000°K and optical depths from 0.1 to 10,000 cm atm. Comparisons with existing experimental data at moderate temperatures and optical depths up to 300 cm atm show satisfactory agreement.

ACKNOWLEDGEMENTS

The authors wish to thank A. Thomson for his many helpful suggestions, D. Brewer and C. N. Abeyta for their assistance in the computations and preparation of the graphs, and F. Oddo for the art work.

REFERENCES

1. C. C. Ferriso, C. B. Ludwig, and F. P. Boynton, "Total Emissivity of Hot Water Vapor, I. The High-Pressure Upper Limit," General Dynamics/Convair, GDA-DBE64-055 (September 1964).
2. G. N. Plass, J. Opt. Soc. Am. 48, 690 (1958).
3. R. M. Goody, Quart. J. Roy. Meteorol. Soc. 78, 165 (1952).
4. C. C. Ferriso, C. B. Ludwig, and A. L. Thomson, "Empirical Infrared Absorption Coefficients of H_2O from 300° to 3000°K," General Dynamics/Convair, GD/C-DBE-65-028 (December 1965).
5. J. N. Howard, D. E. Burch, and D. Williams, J. Opt. Soc. Am. 46, 242, 334 (1956).
6. H. C. Hottel and R. B. Egbert, Am. Inst. Chem. Eng. 38, 531 (1942).
7. D. K. Edwards, B. J. Flornes, L. K. Glassen, and W. Sun, Appl. Opt. 4, 715 (1965).
8. D. E. Burch and D. A. Gryvnak, "Infrared Radiation Emitted by Hot Gases and Its Transmission through Synthetic Atmospheres," Ford Motor Company, Aeronutronics Division, U-1929 (October 1962).
9. W. Malkmus, "Random Lorentz Band Model with Exponential-Tailed S^{-1} Line Intensity Distribution Function," General Dynamics/Convair, GD/C-DBE-65-020 (November 1965).
10. D. E. Burch, E. B. Singleton, and D. Williams, Appl. Opt. 1, 359 (1962).
11. K. E. Nelson, "Experimental Determination of the Band Absorptivities of Water Vapor at Elevated Pressures and Temperatures," M. S. Thesis, University of California (1959).
12. L. D. Gray, Ph.D. Thesis, California Institute of Technology, Pasadena, California (1963).

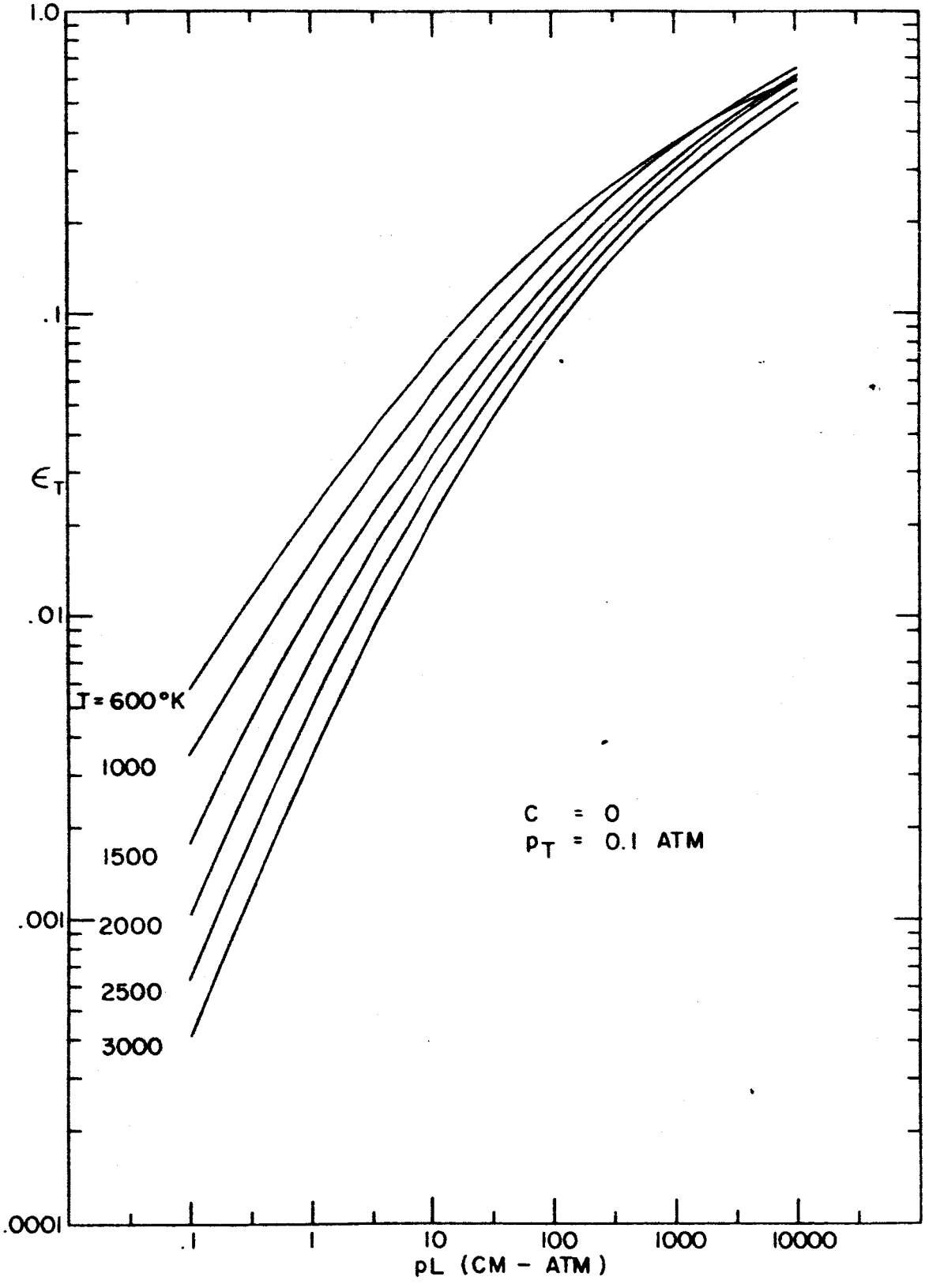

Fig. 1. Total emissivity versus optical depth for zero partial pressure of water at a total pressure of 0.1 atm.

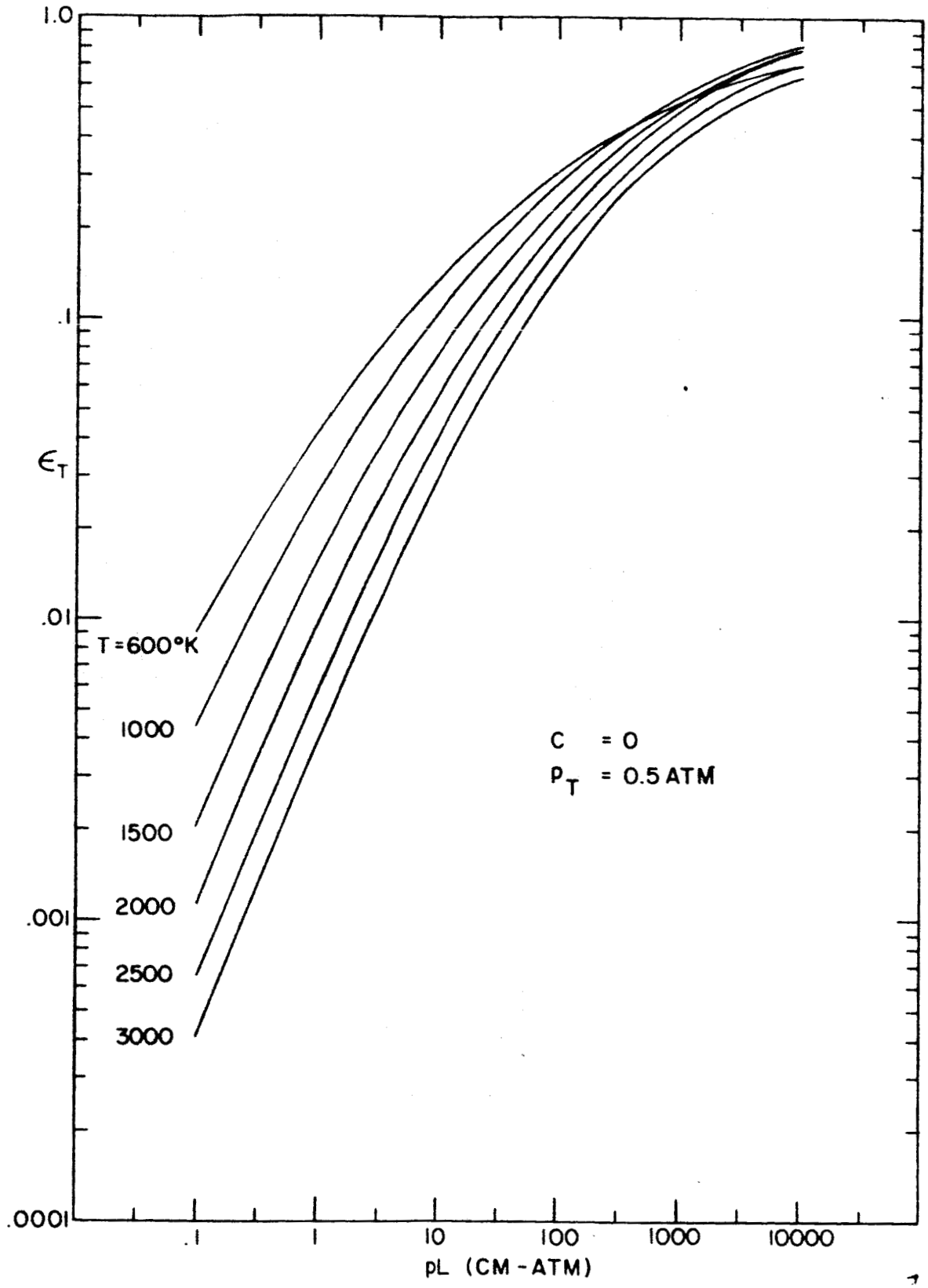

Fig. 2. Total emissivity versus optical depth for zero partial pressure of water at a total pressure of 0.5 atm.

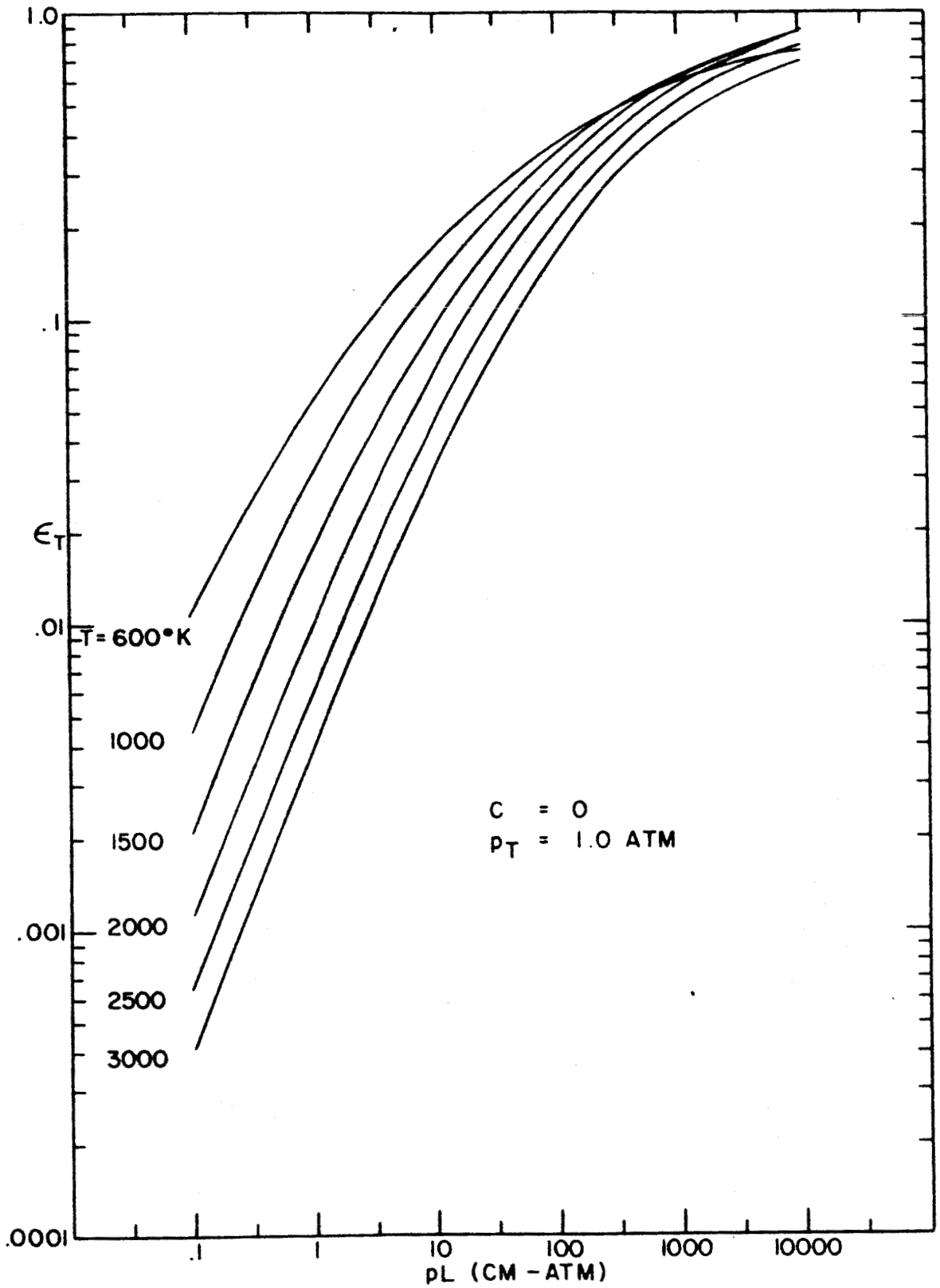

Fig. 3. Total emissivity versus optical depth for zero partial pressure of water at a total pressure of 1 atm.

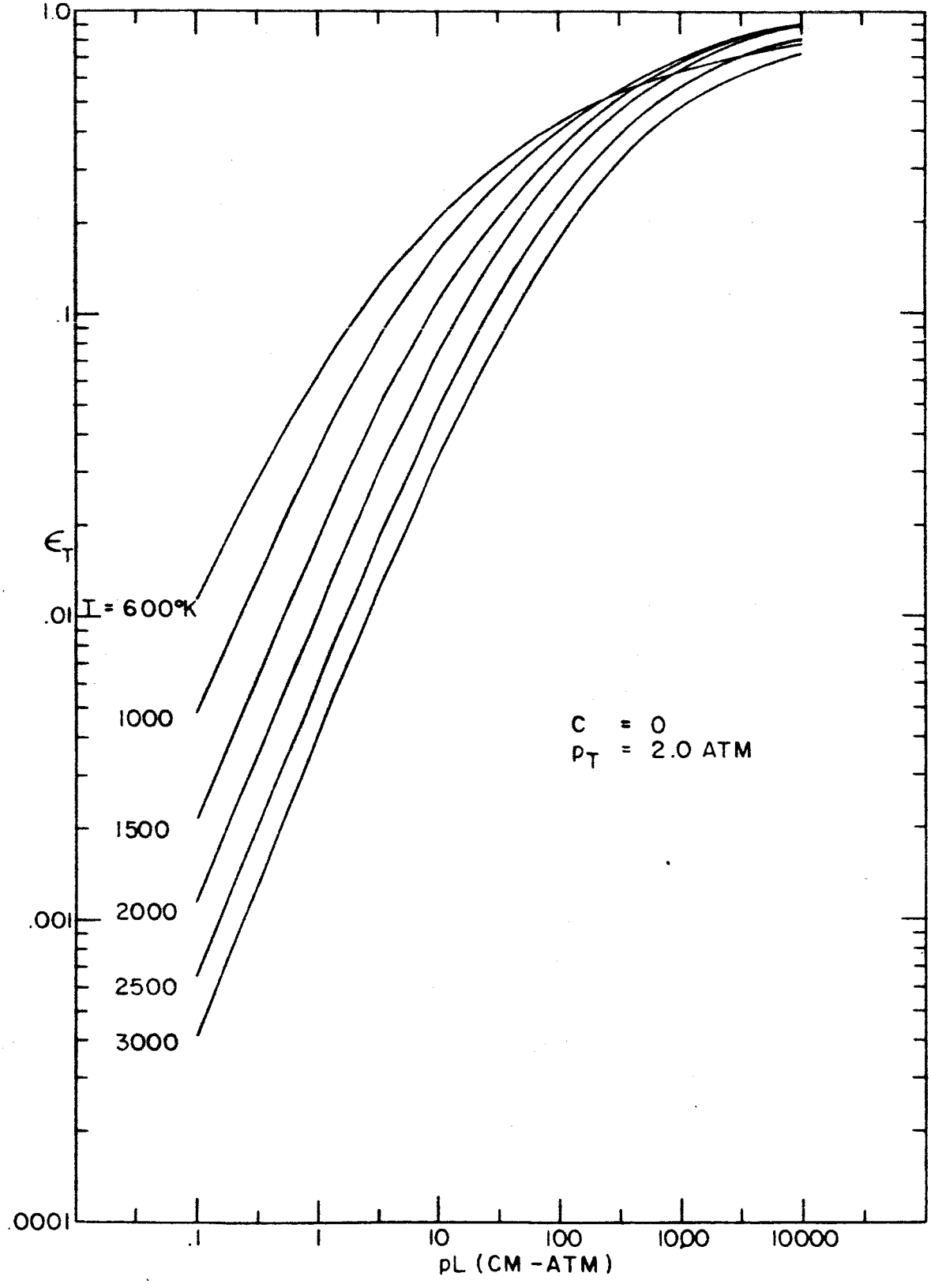

Fig. 4. Total emissivity versus optical depth for zero partial pressure of water at a total pressure of 2 atm.

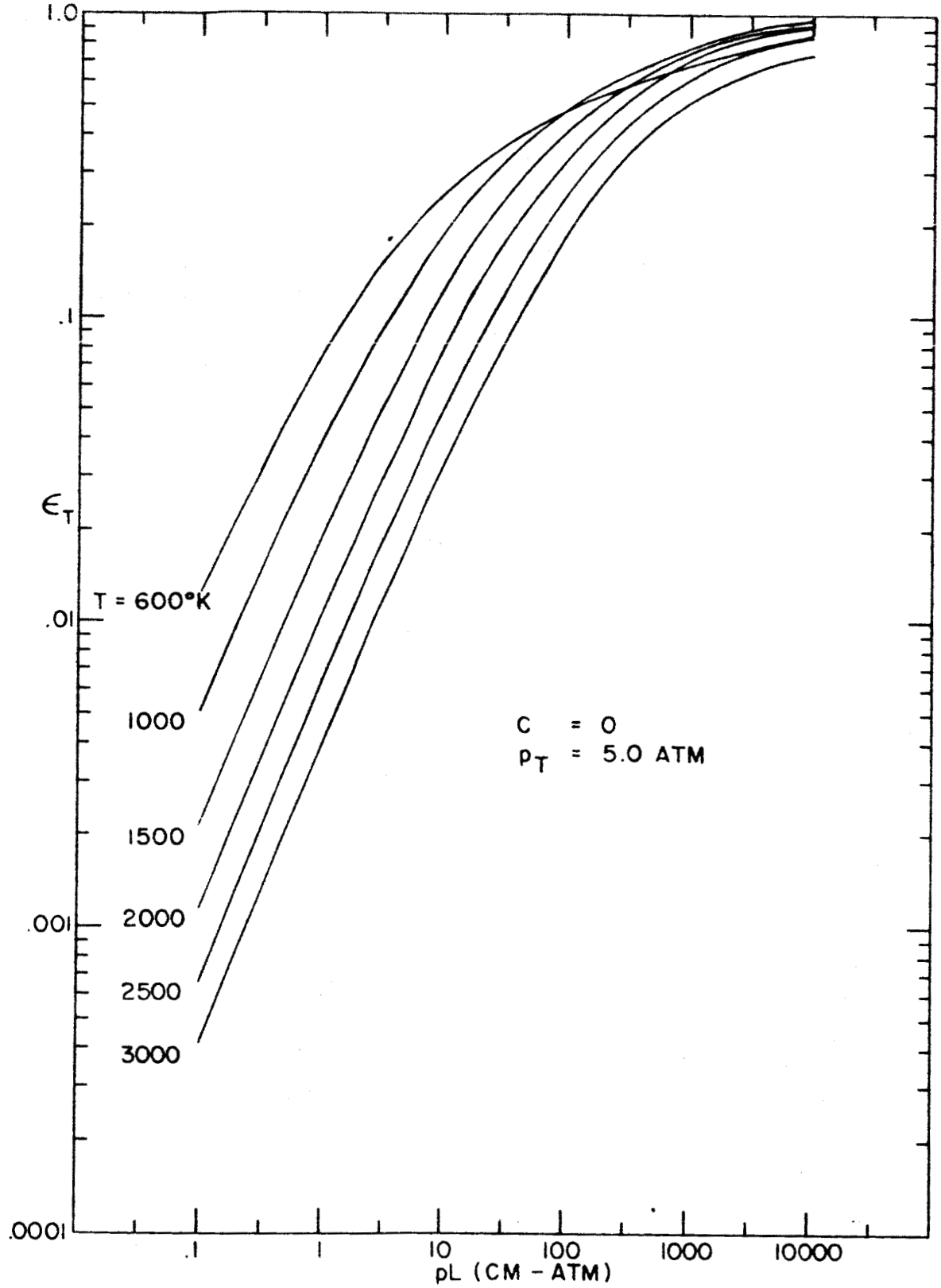

Fig. 5. Total emissivity versus optical depth for zero partial pressure of water at a total pressure of 5 atm.

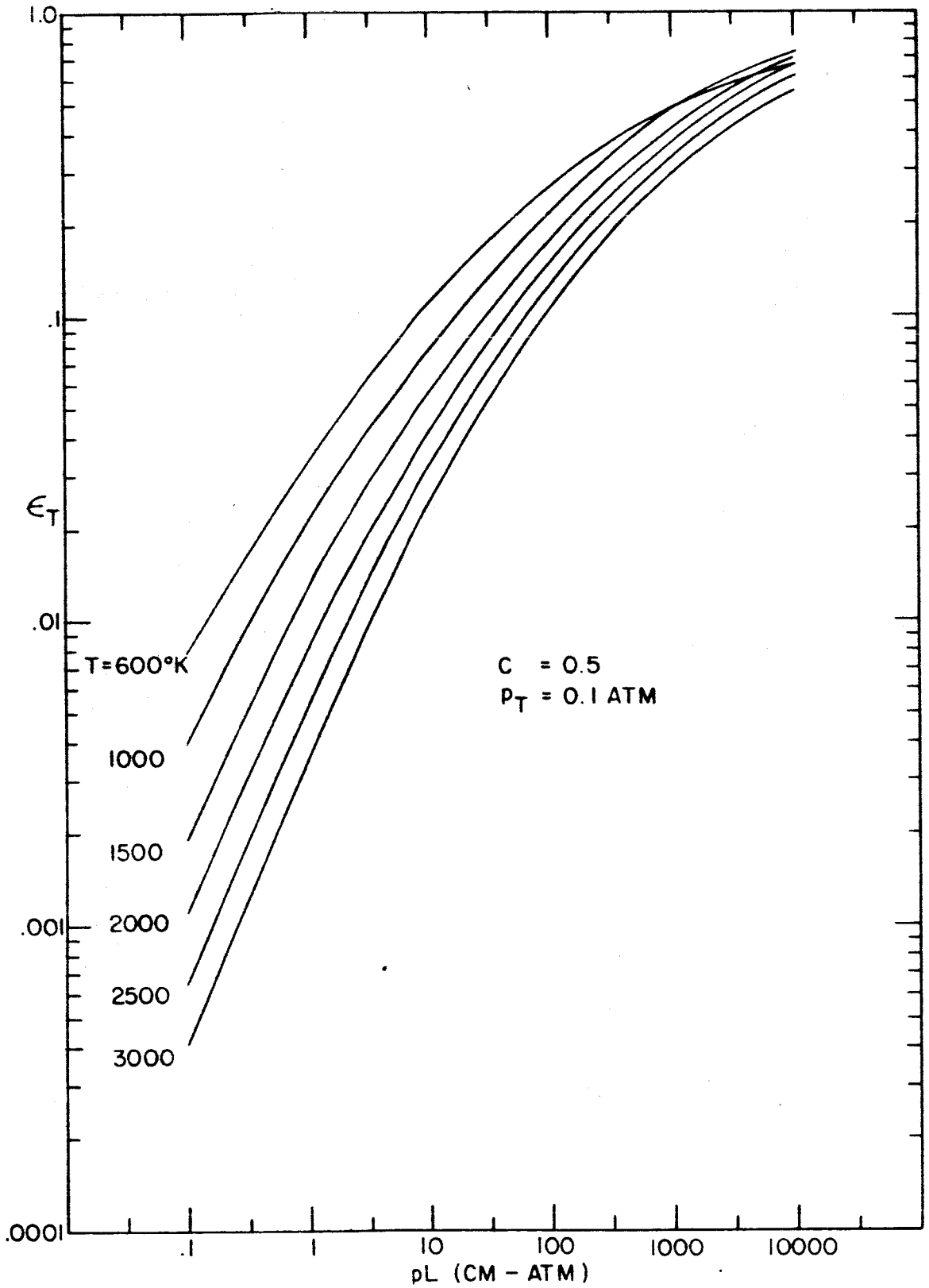

Fig. 6. Total emissivity versus optical depth for a mixture of 50% water and 50% N_2 (mole concentration) at a total pressure of 0.1 atm.

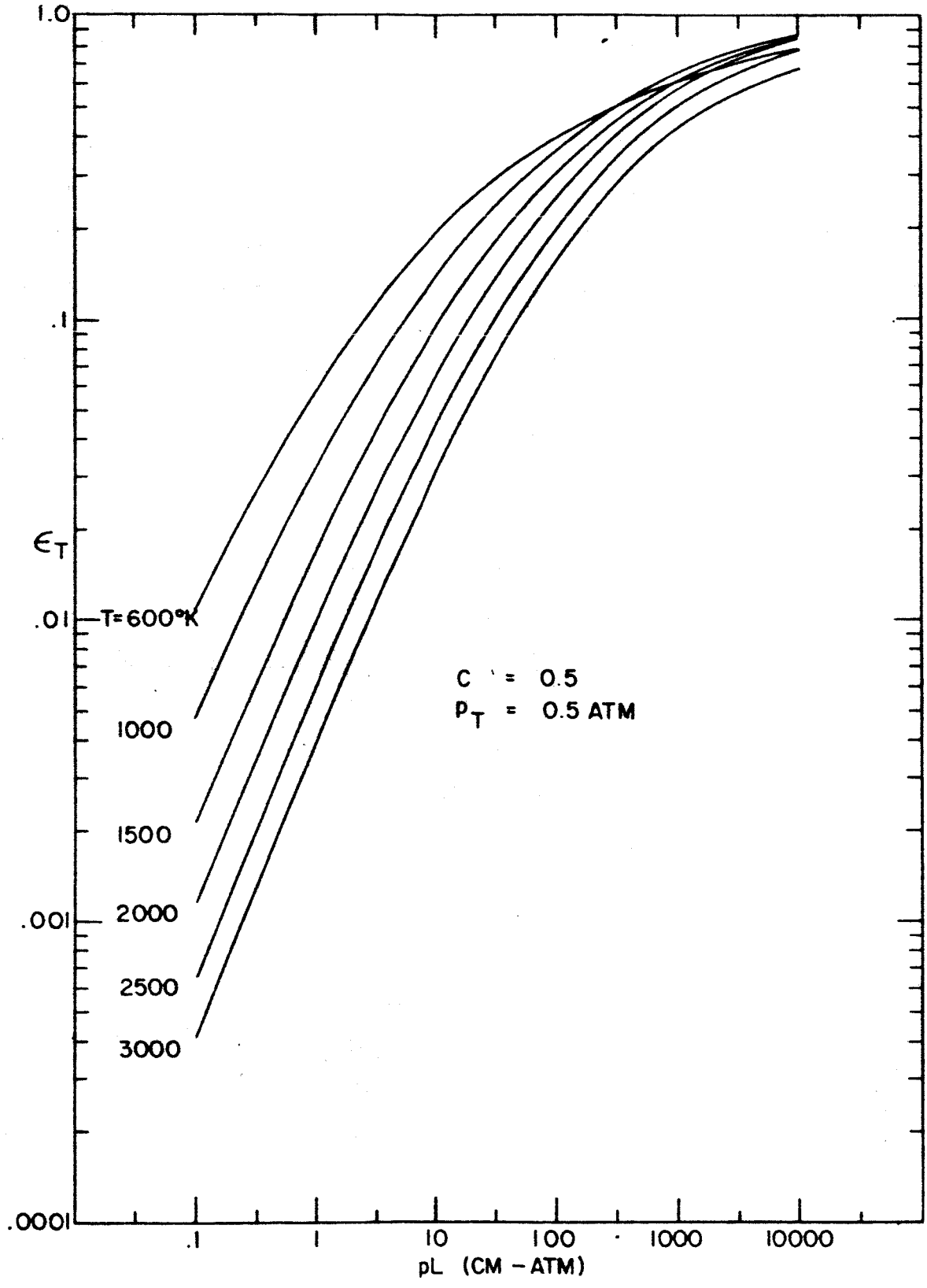

Fig. 7. Total emissivity versus optical depth for a mixture of 50% water and 50% N_2 (mole concentration) at a total pressure of .5 atm.

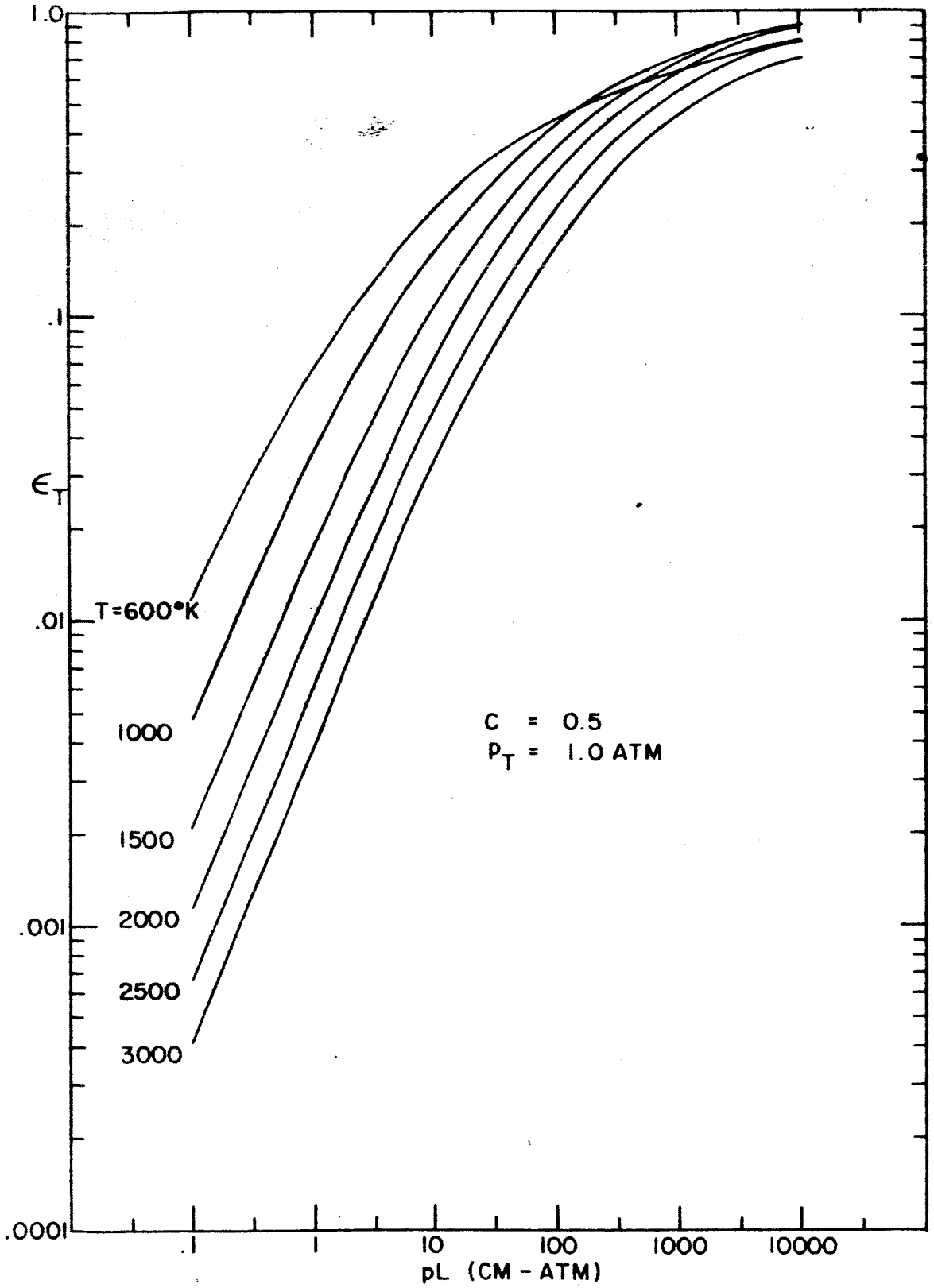

Fig. 8. Total emissivity versus optical depth for a mixture of 50% water and 50% N_2 (mole concentration) at a total pressure of 1 atm.

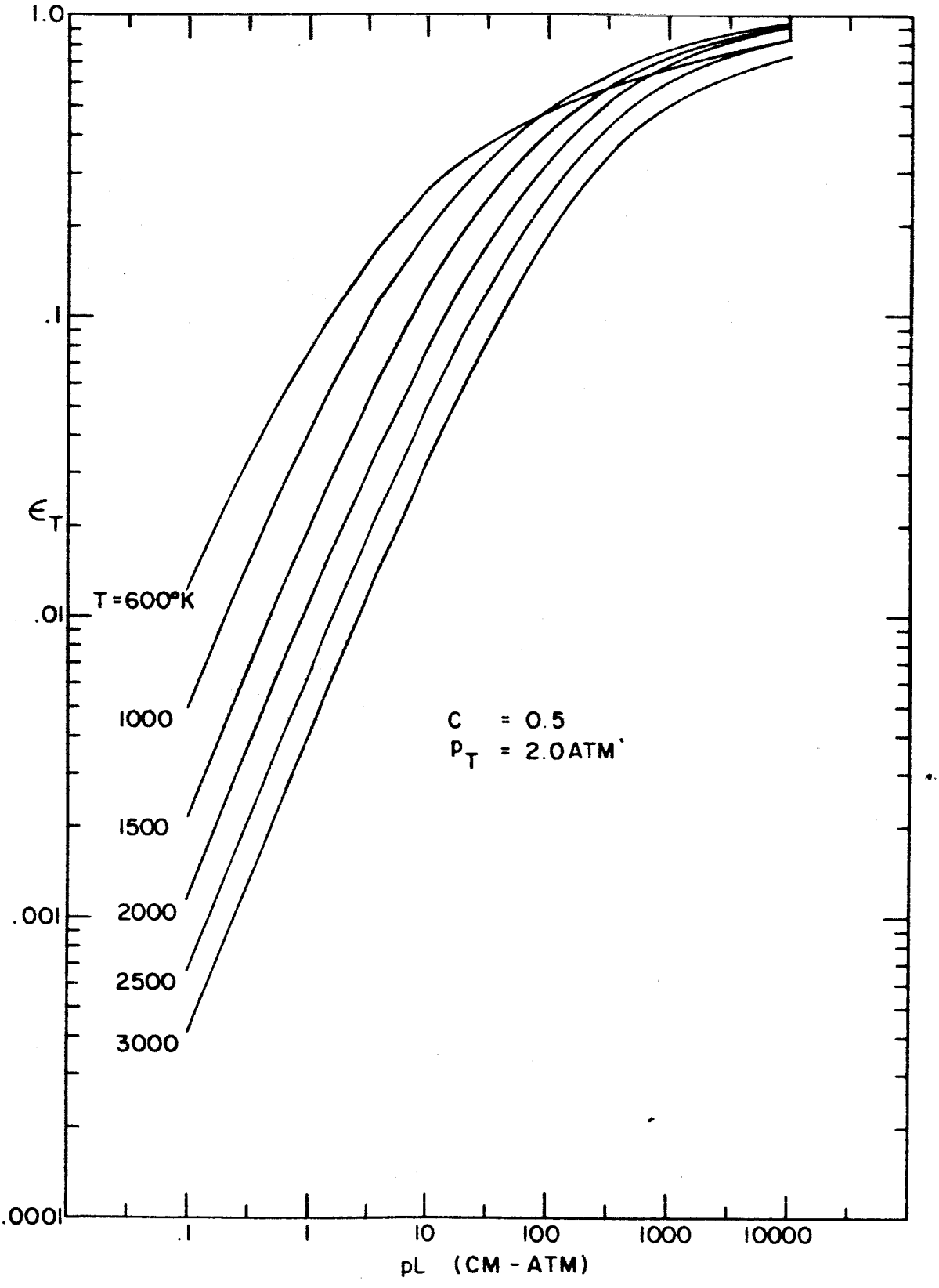

Fig. 9. Total emissivity versus optical depth for a mixture of 50% water and 50% N_2 (mole concentration) at a total pressure of 2 atm.

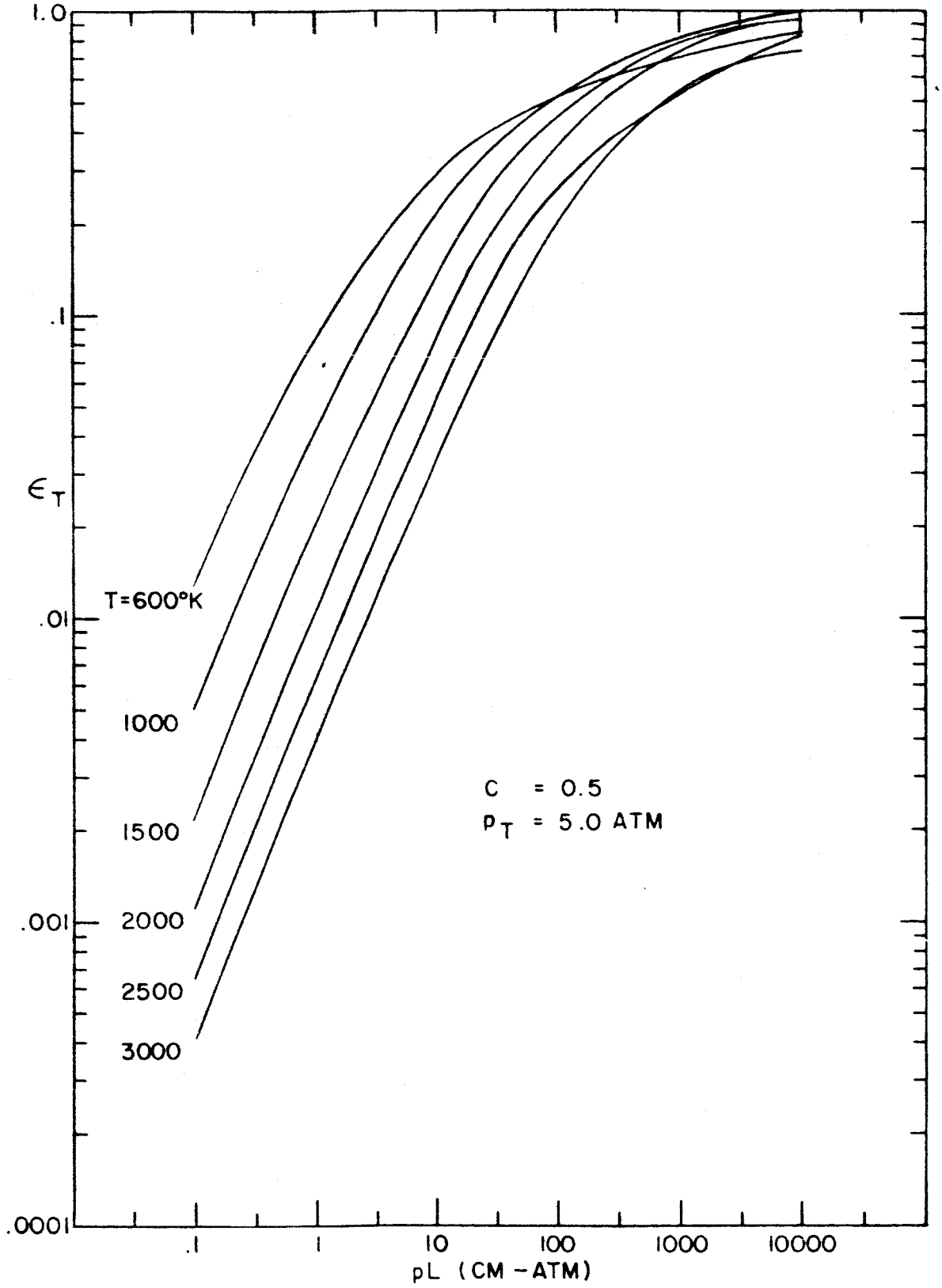

Fig. 10. Total emissivity versus optical depth for a mixture of 50% water and 50% N_2 (mole concentration) at a total pressure of 5 atm.

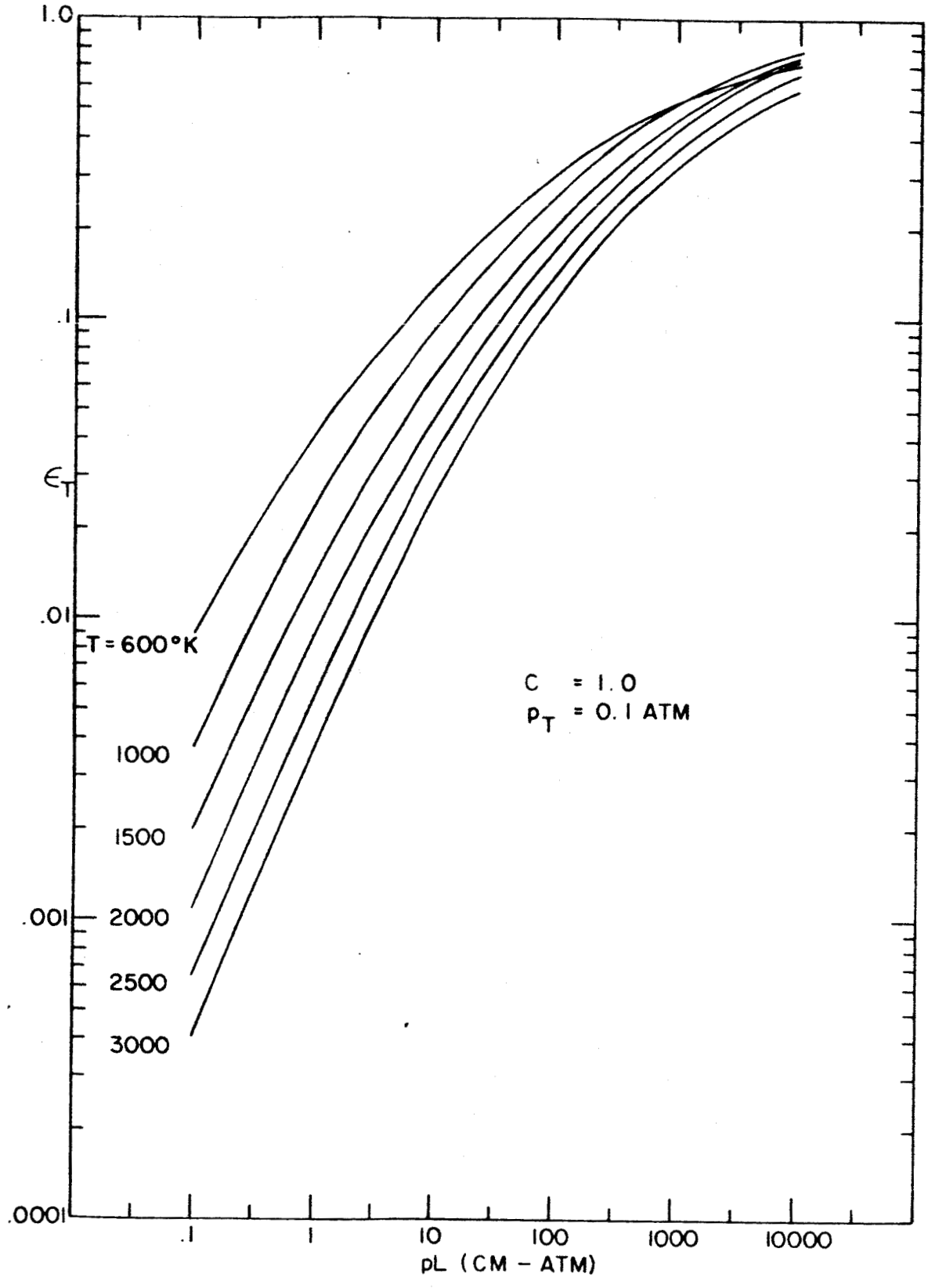

Fig. 11. Total emissivity versus optical depth for pure water at a total pressure of 0.1 atm.

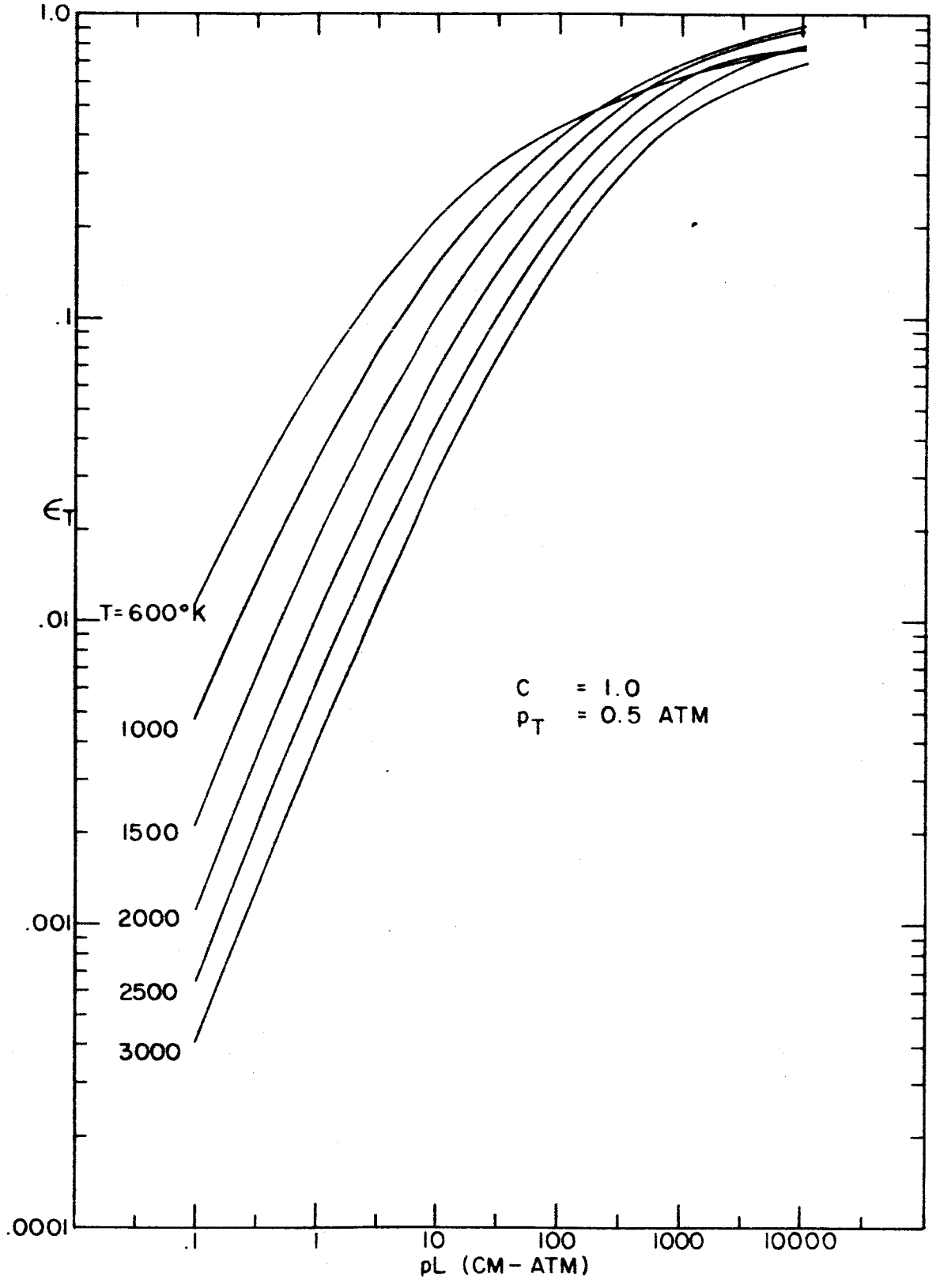

Fig. 12. Total emissivity versus optical depth for pure water at a total pressure of .5 atm.

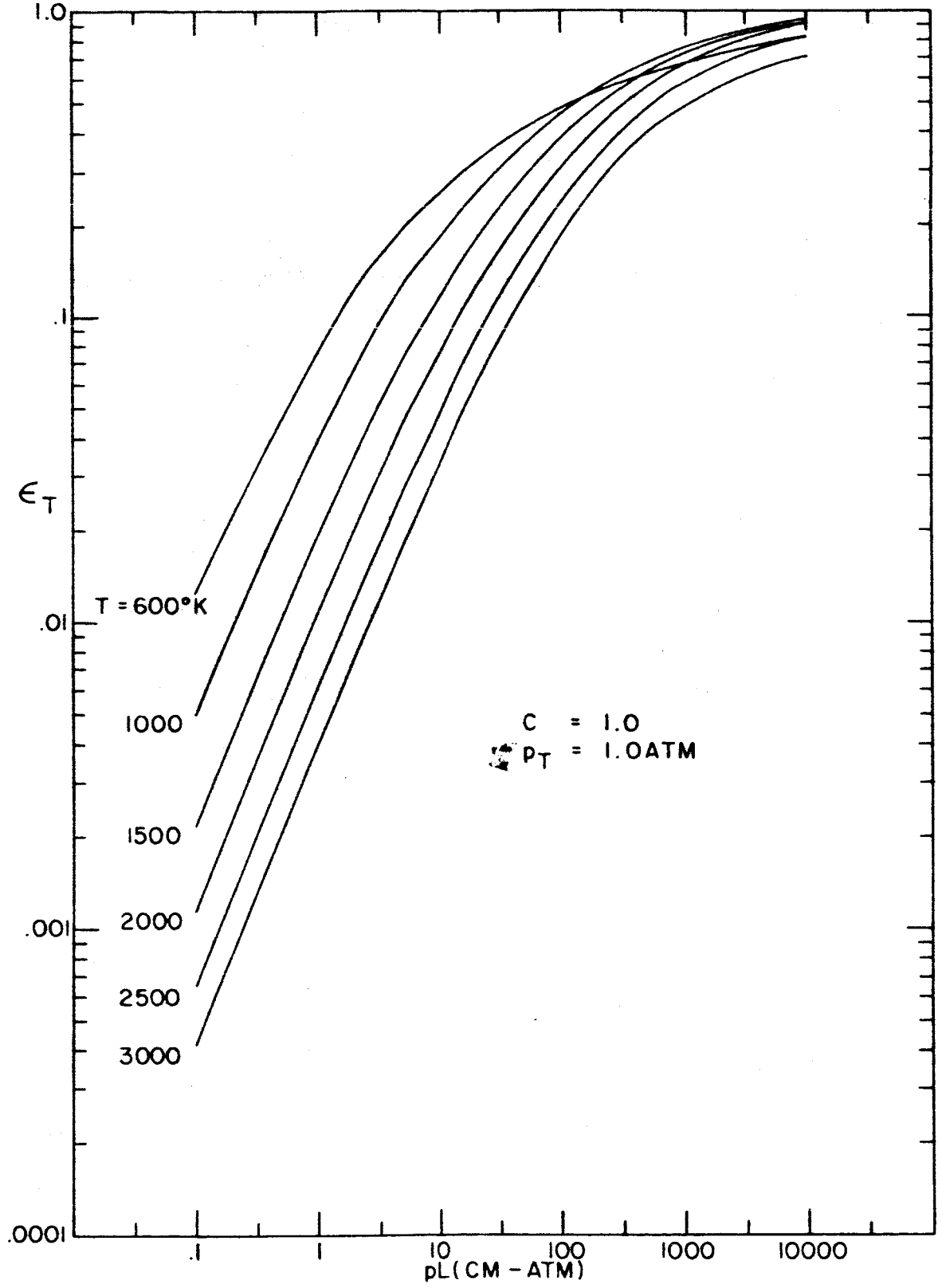

Fig. 13. Total emissivity versus optical depth for pure water at a total pressure of 1 atm.

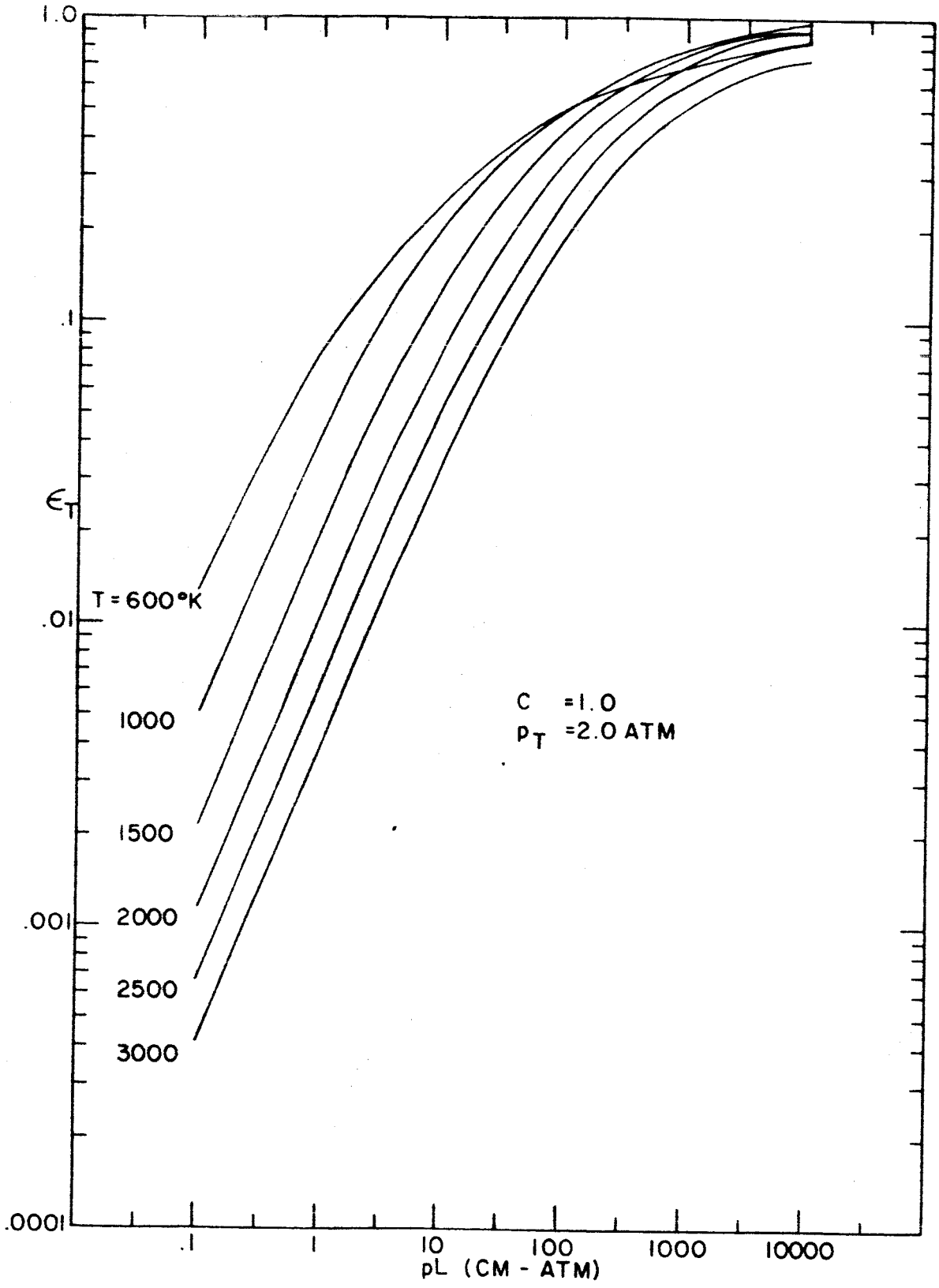

Fig. 14. Total emissivity versus optical depth for pure water at a total pressure of 2 atm.

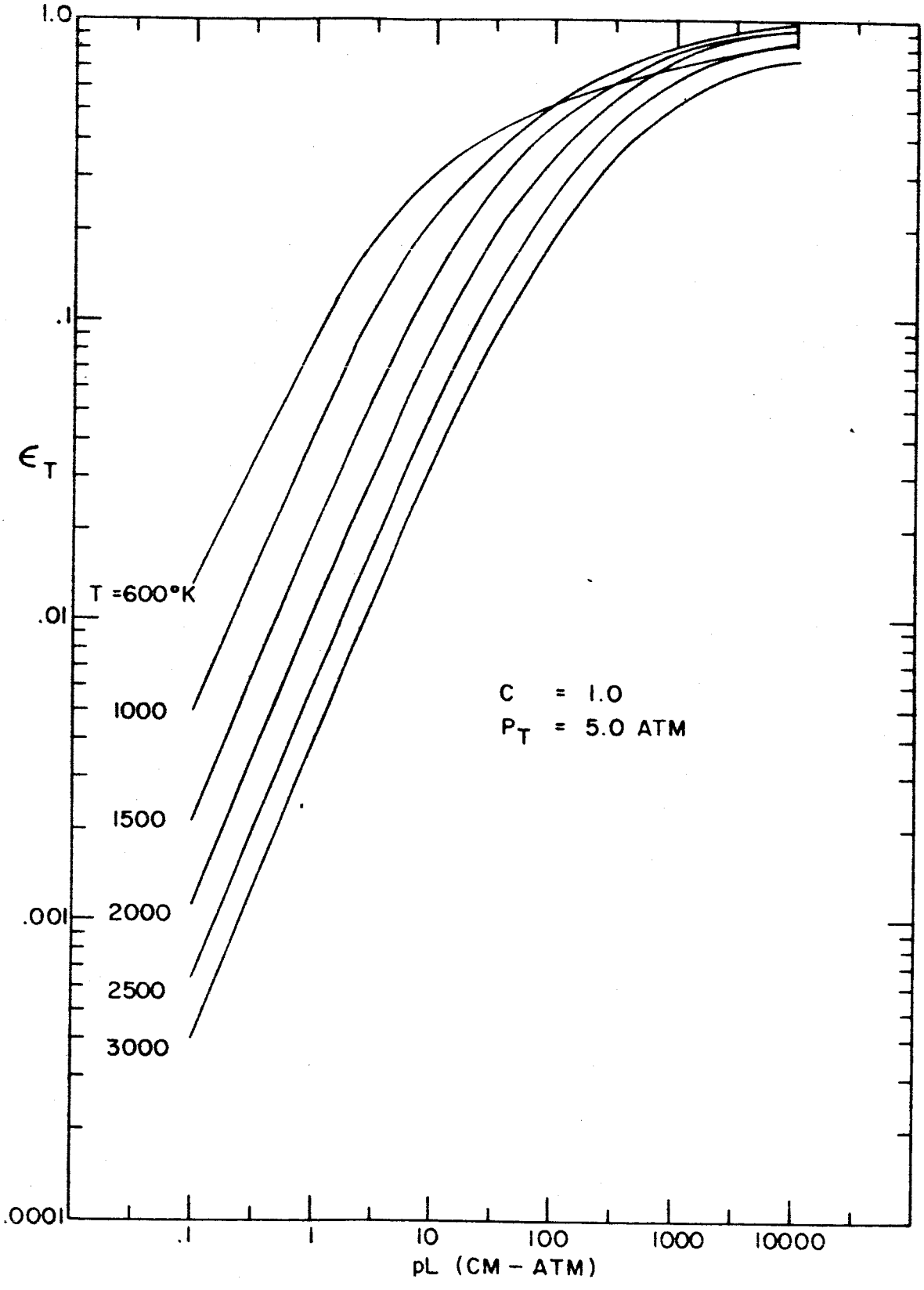

Fig. 15. Total emissivity versus optical depth for pure water at a total pressure of 5 atm.

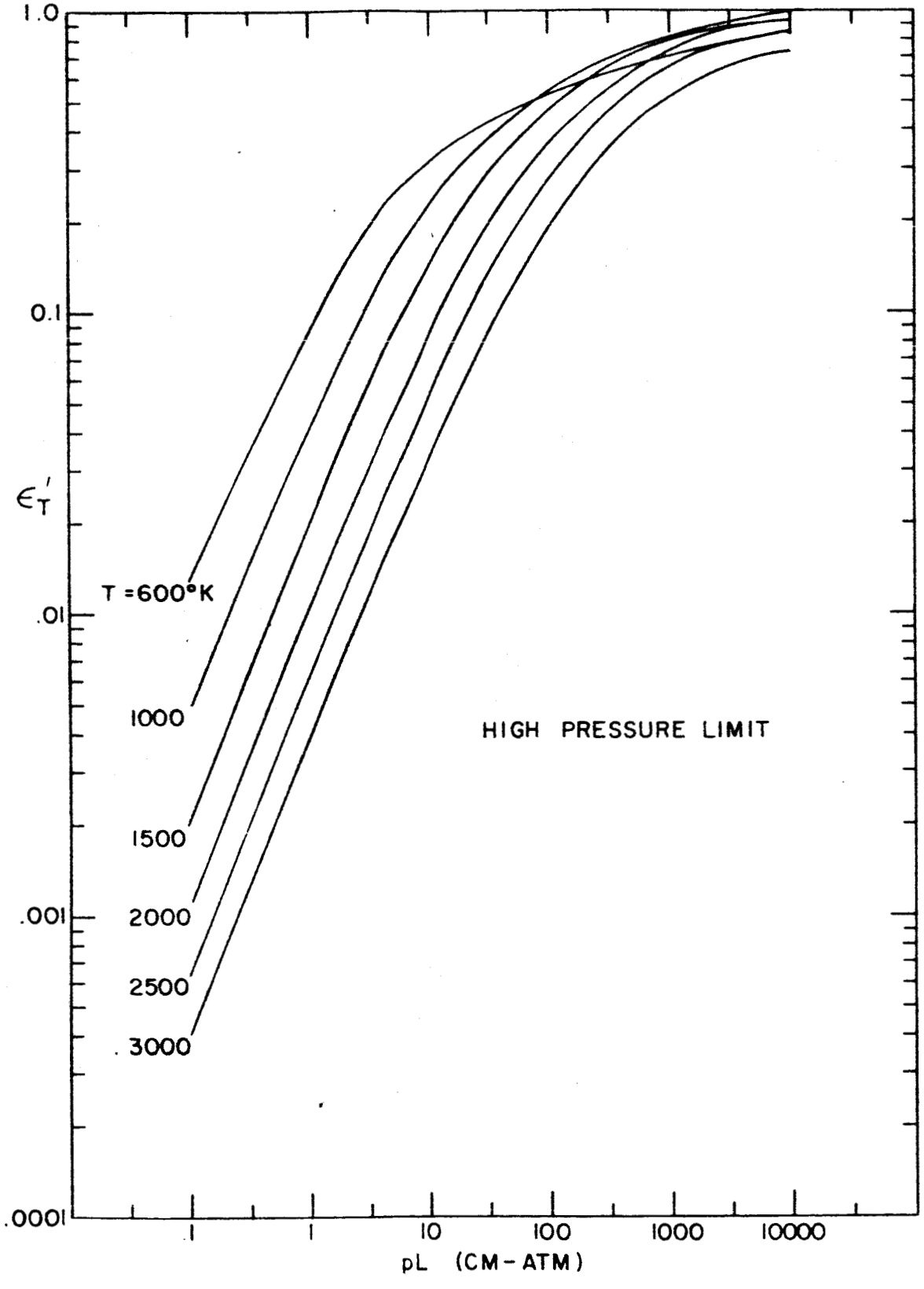

Fig. 16. Total emissivity of water versus optical depth at the high pressure limit.

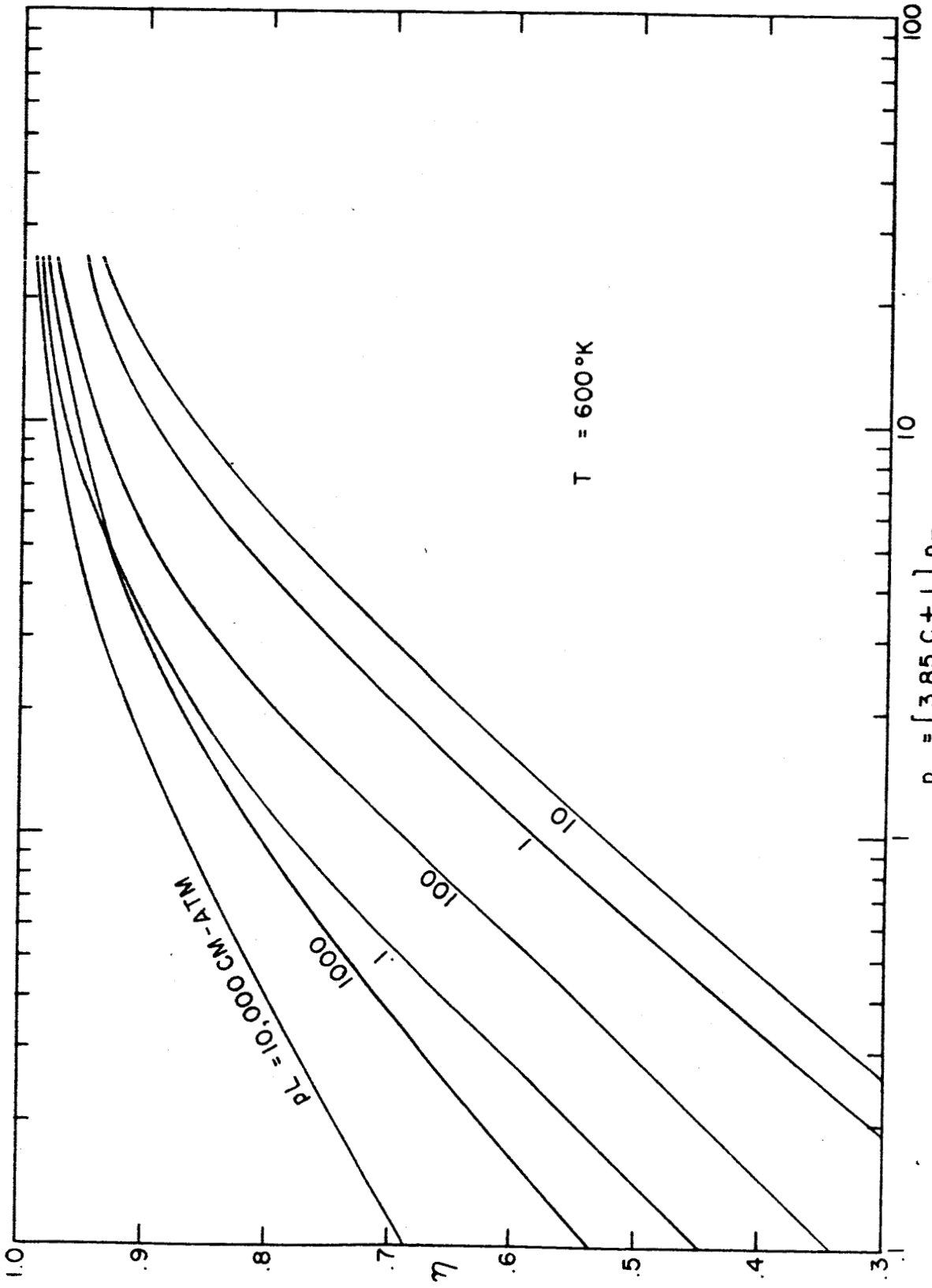

Fig. 17. The ratio η versus equivalent pressure at 600°K.

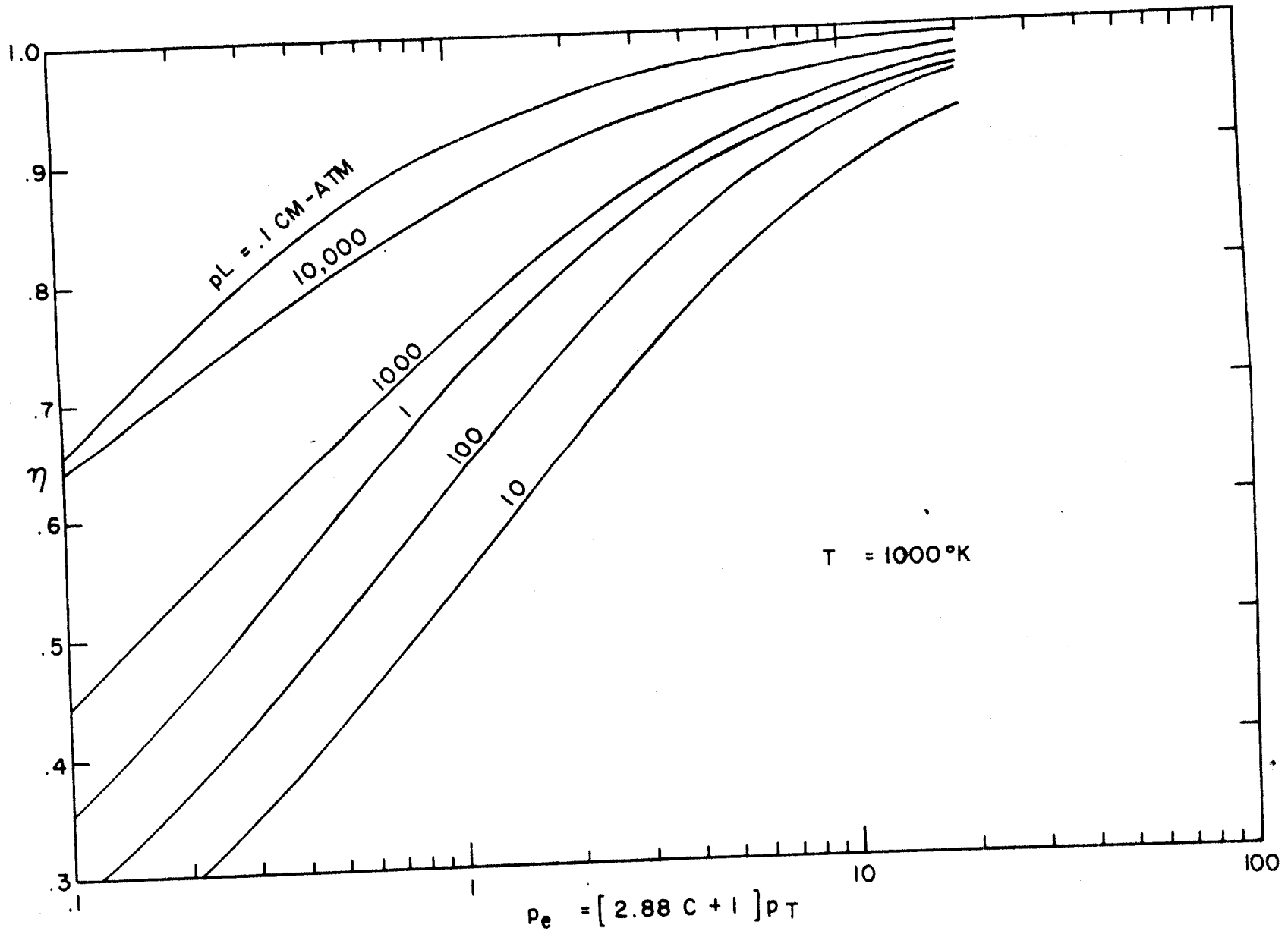

Fig. 18. The ratio η versus equivalent pressure at 1000°K.

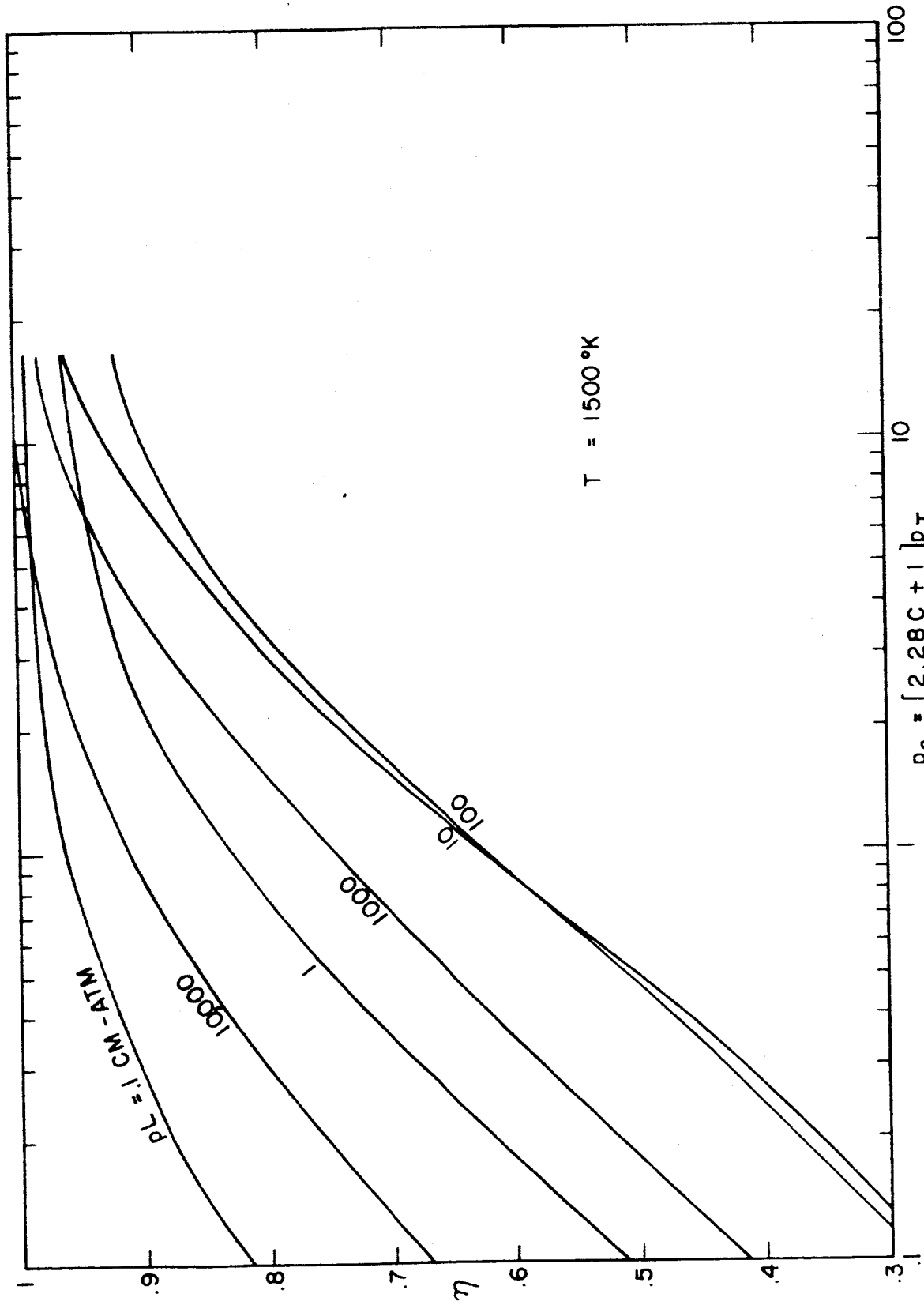

Fig. 19. The ratio η versus equivalent pressure at 1500°K.

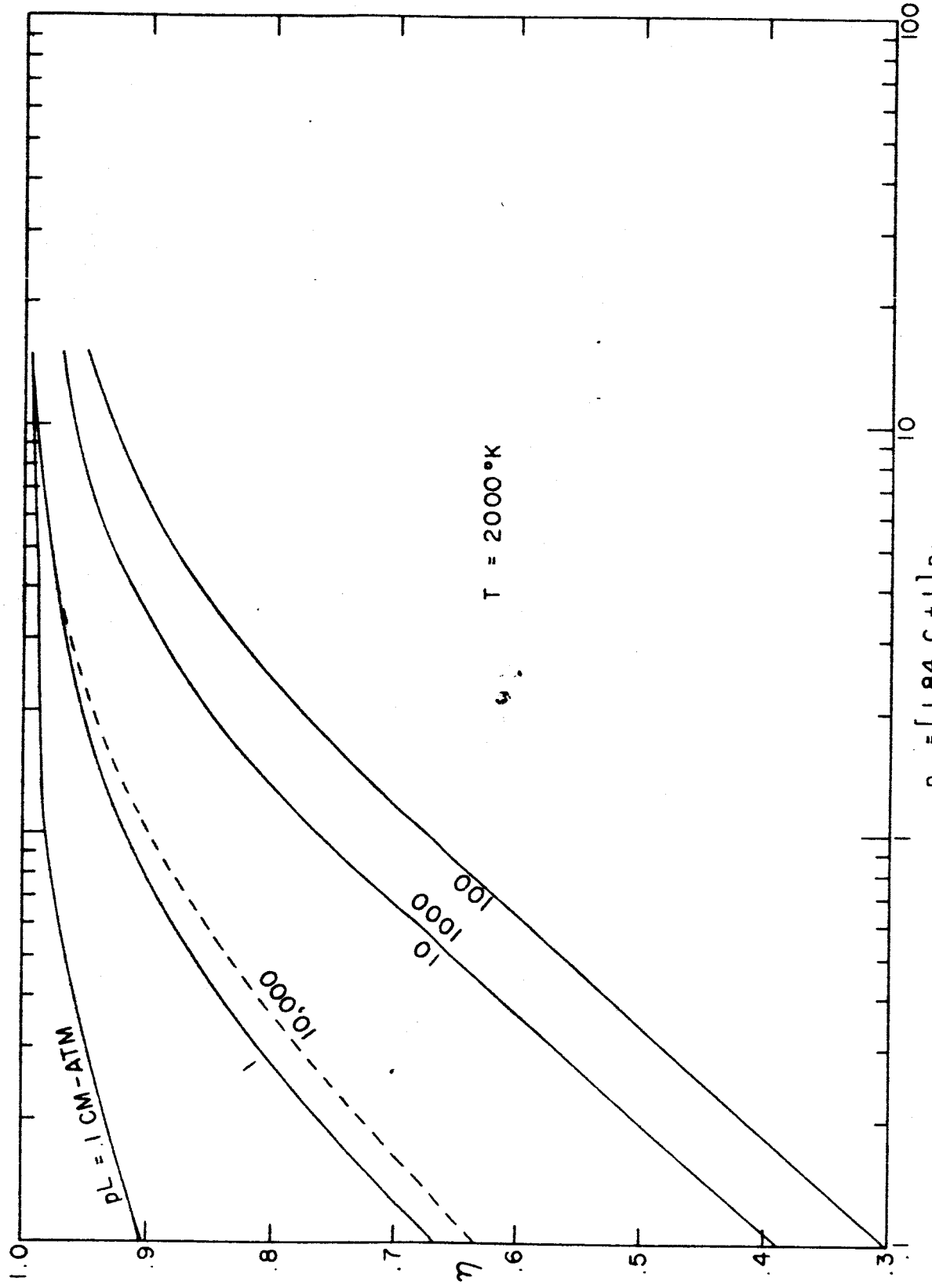

Fig. 20. The ratio η versus equivalent pressure at 2000°K.

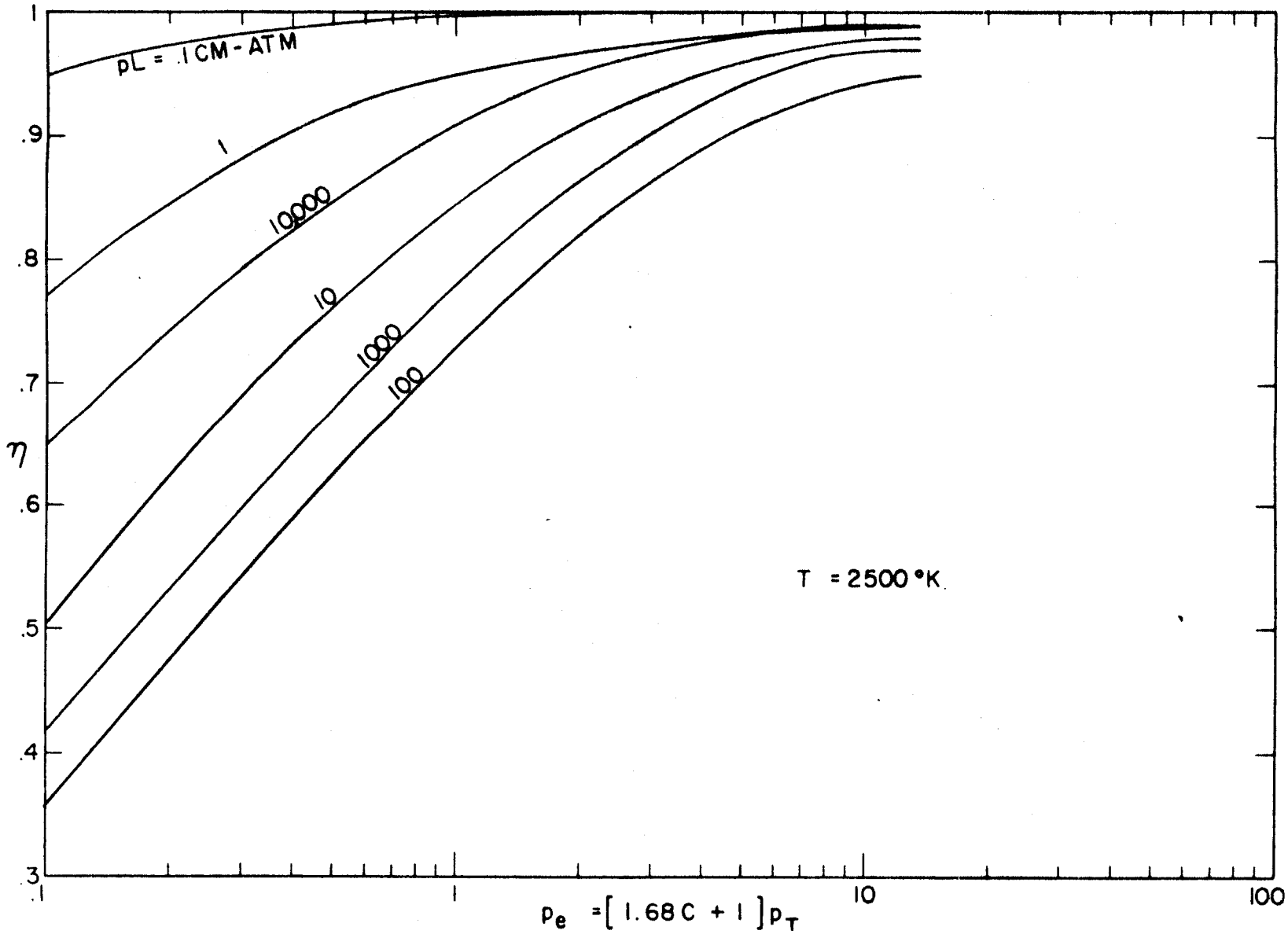

Fig. 21. The ratio η versus equivalent pressure at 2500°K.

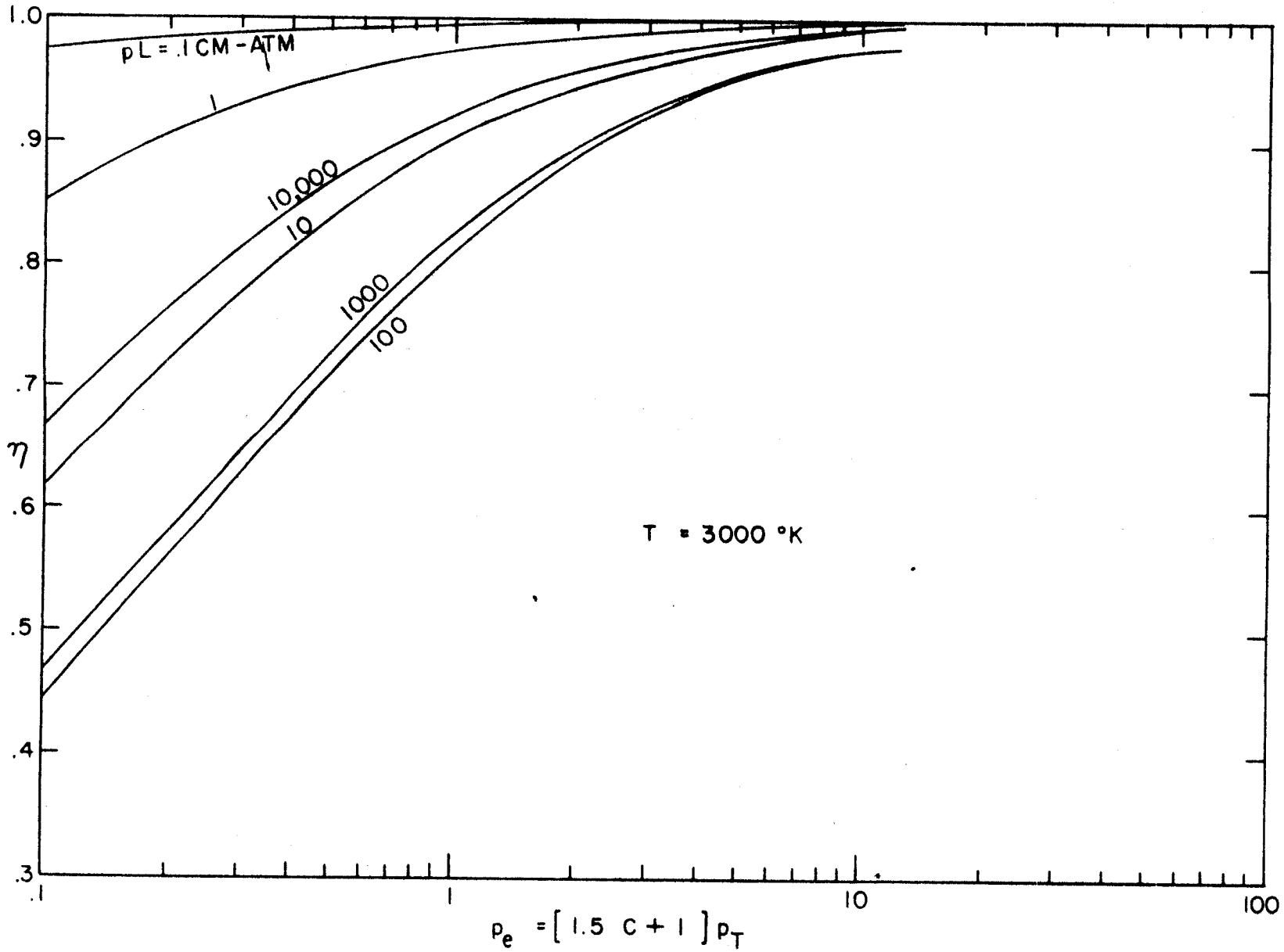

Fig. 22. The ratio η versus equivalent pressure at 3000°K.

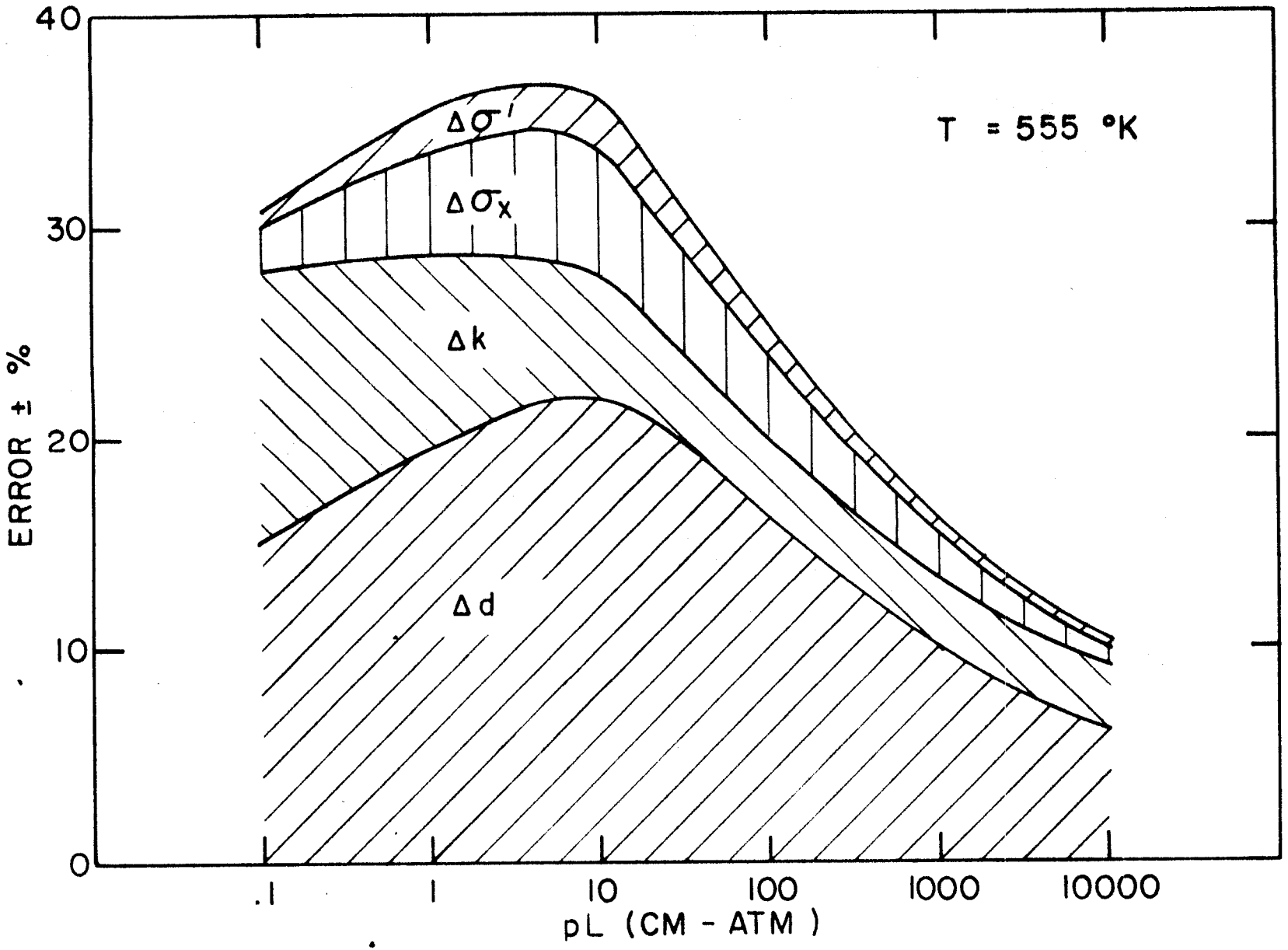

Fig. 23. Computed error in total emissivity at 555°K for $\Delta d = \pm 100\%$, $\Delta k = \pm 20\%$, $\Delta\sigma_x = \pm 20\%$, and $\sigma' = \pm 100\%$.

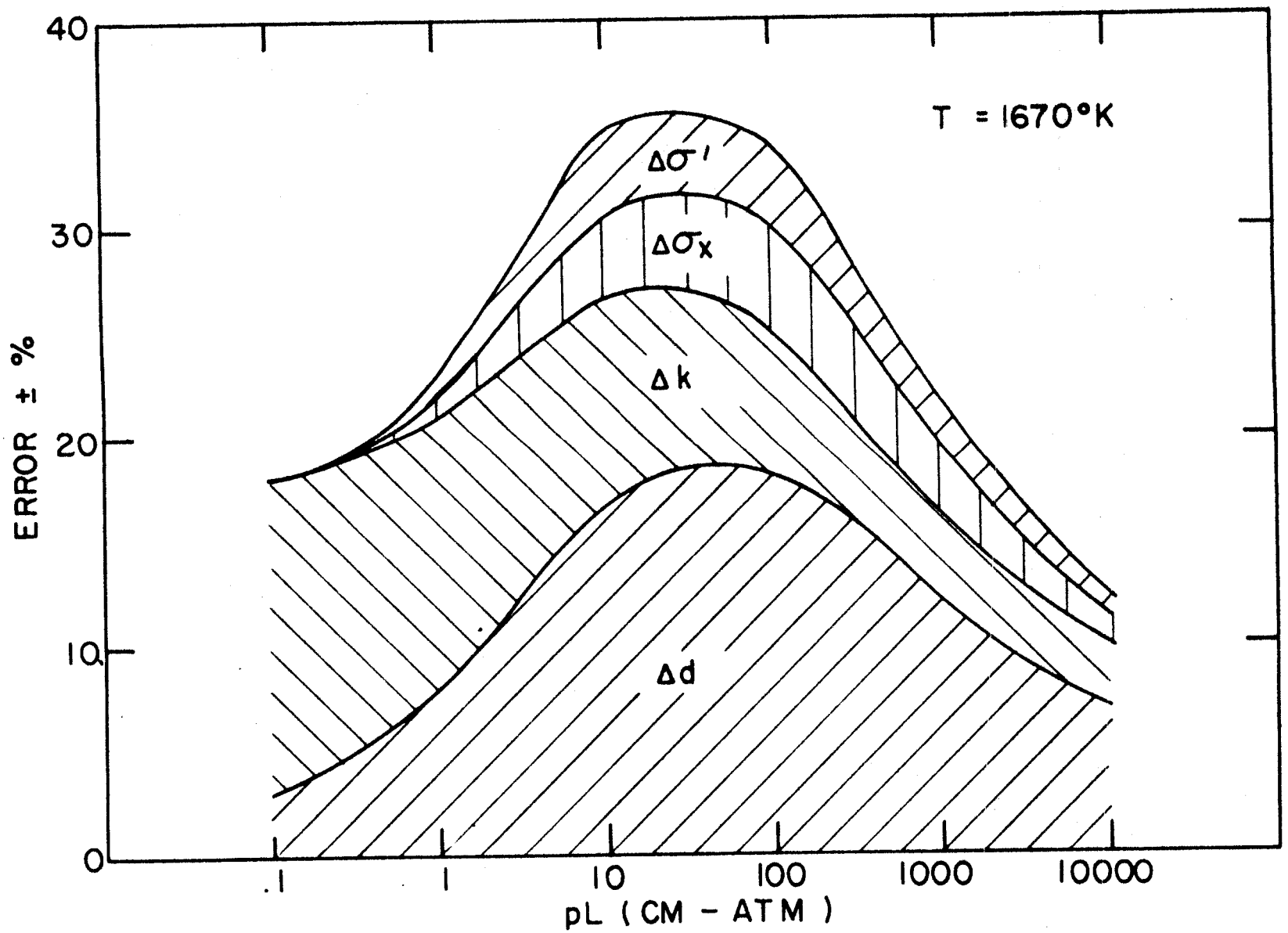

Fig. 24. Computed error in total emissivity at 1670°K for $\Delta d = \pm 100\%$, $\Delta k = \pm 20\%$, $\Delta\sigma_x = \pm 20\%$, and $\sigma' = \pm 100\%$.

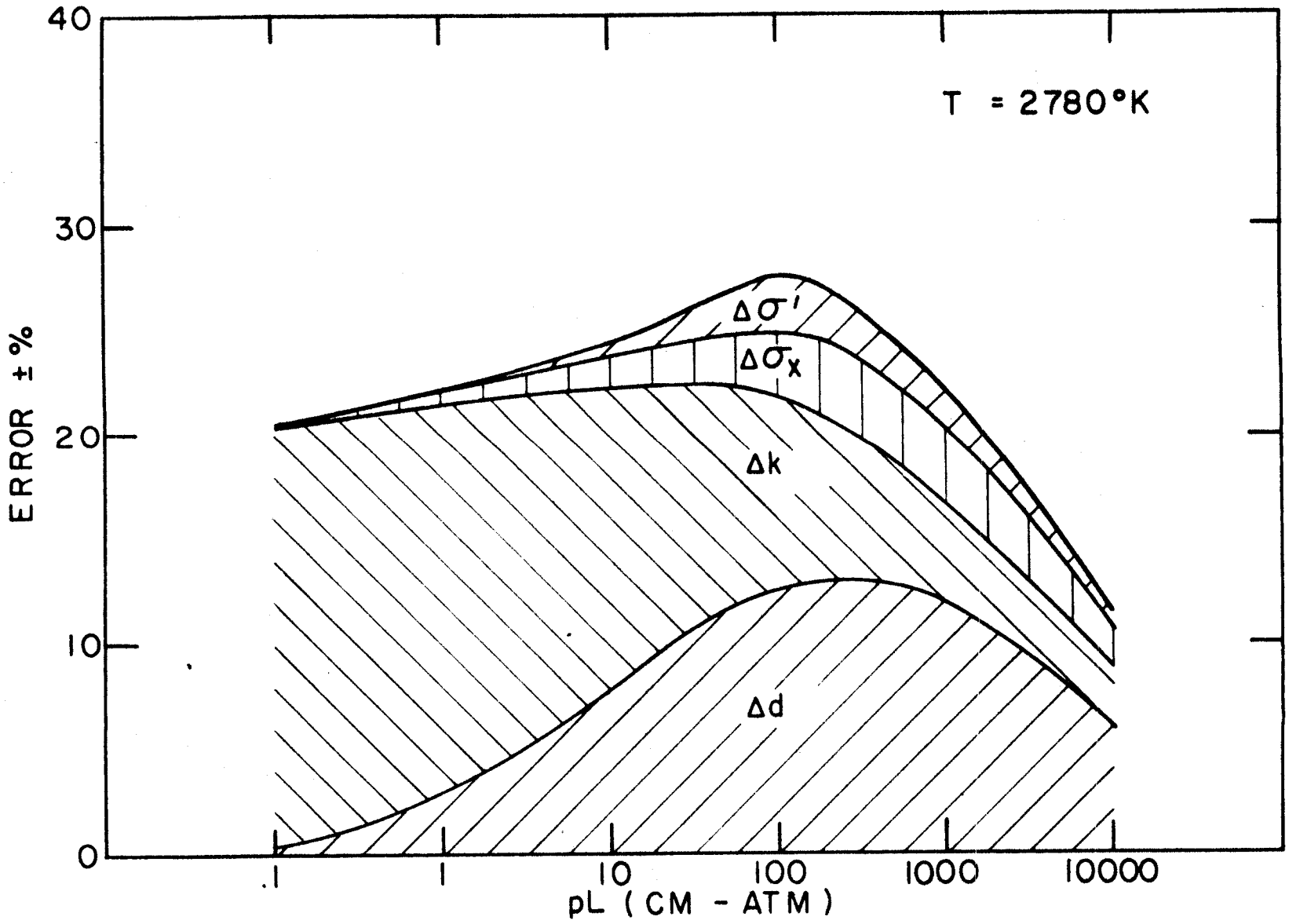

Fig. 25. Computed error in total emissivity at 2780°K for $\Delta d = \pm 100\%$, $\Delta k = \pm 20\%$, $\Delta\sigma_x = \pm 20\%$, and $\sigma' = \pm 100\%$.

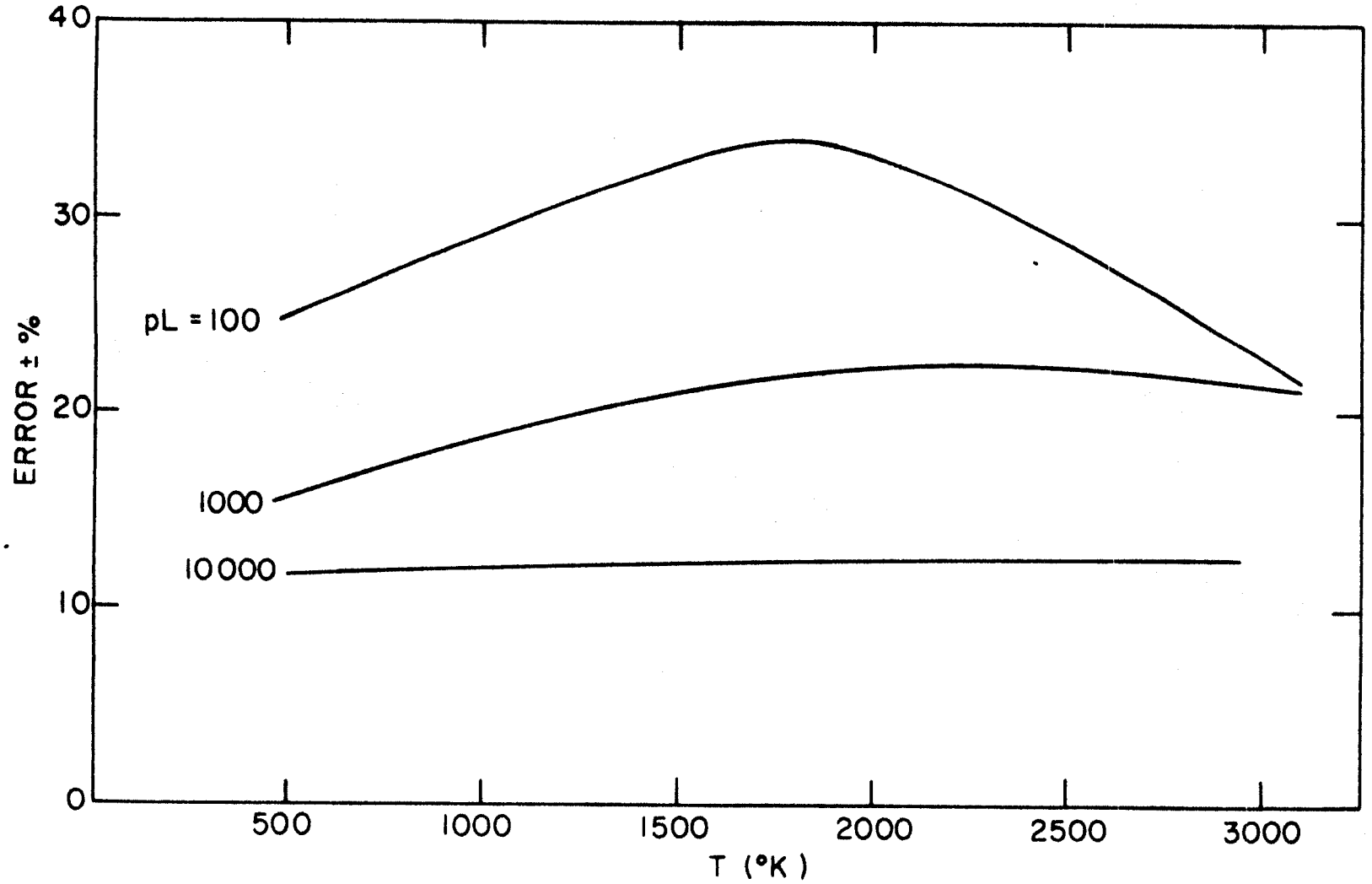

Fig. 26. Total computed error versus temperature for optical depths equal to 100, 1000, and 10,000 cm atm.

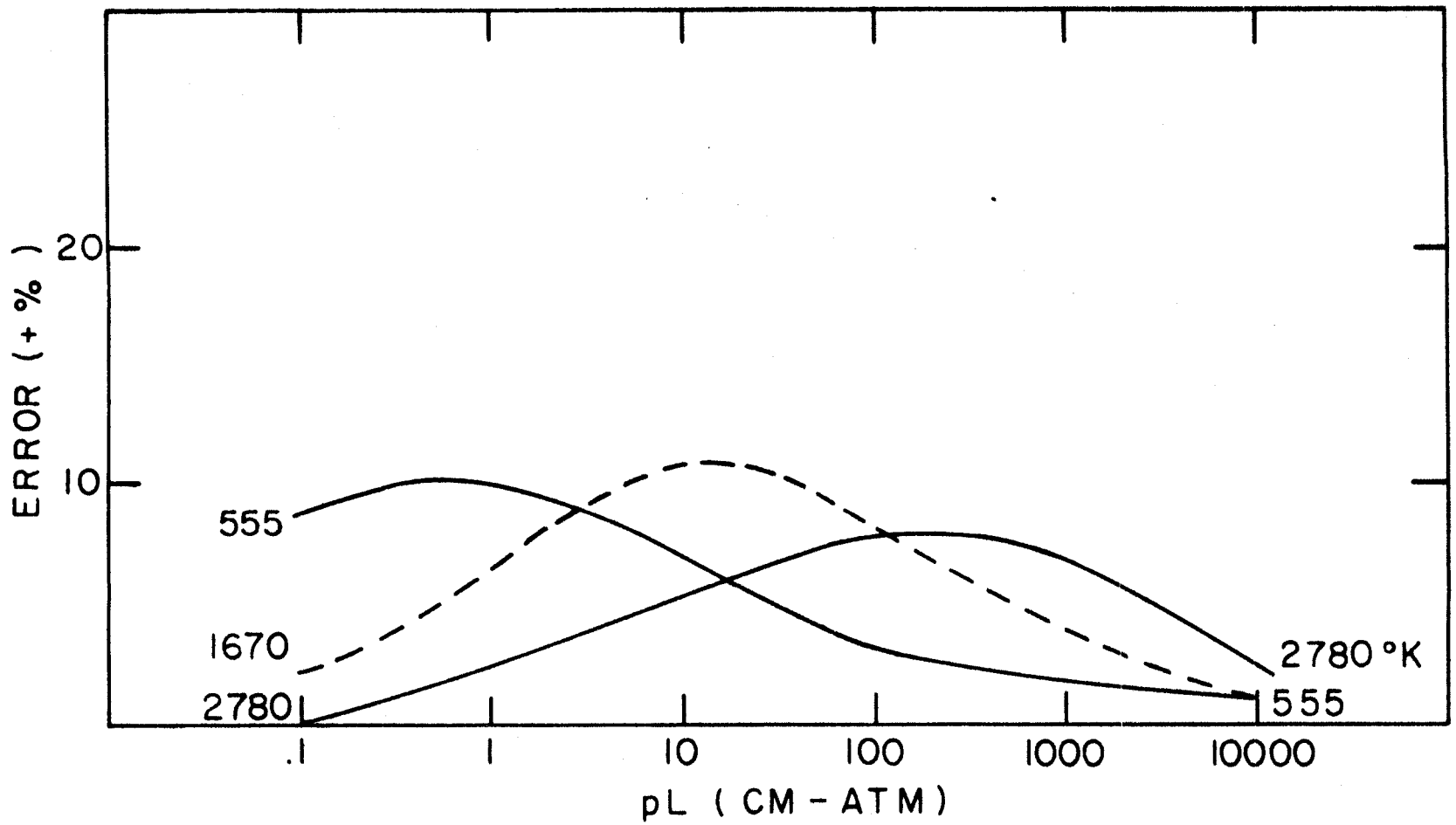

Fig. 27. Total computed error versus optical depth for temperatures equal to 555°, 1670°, and 2780°K due to the line intensity distribution S^{-1}.

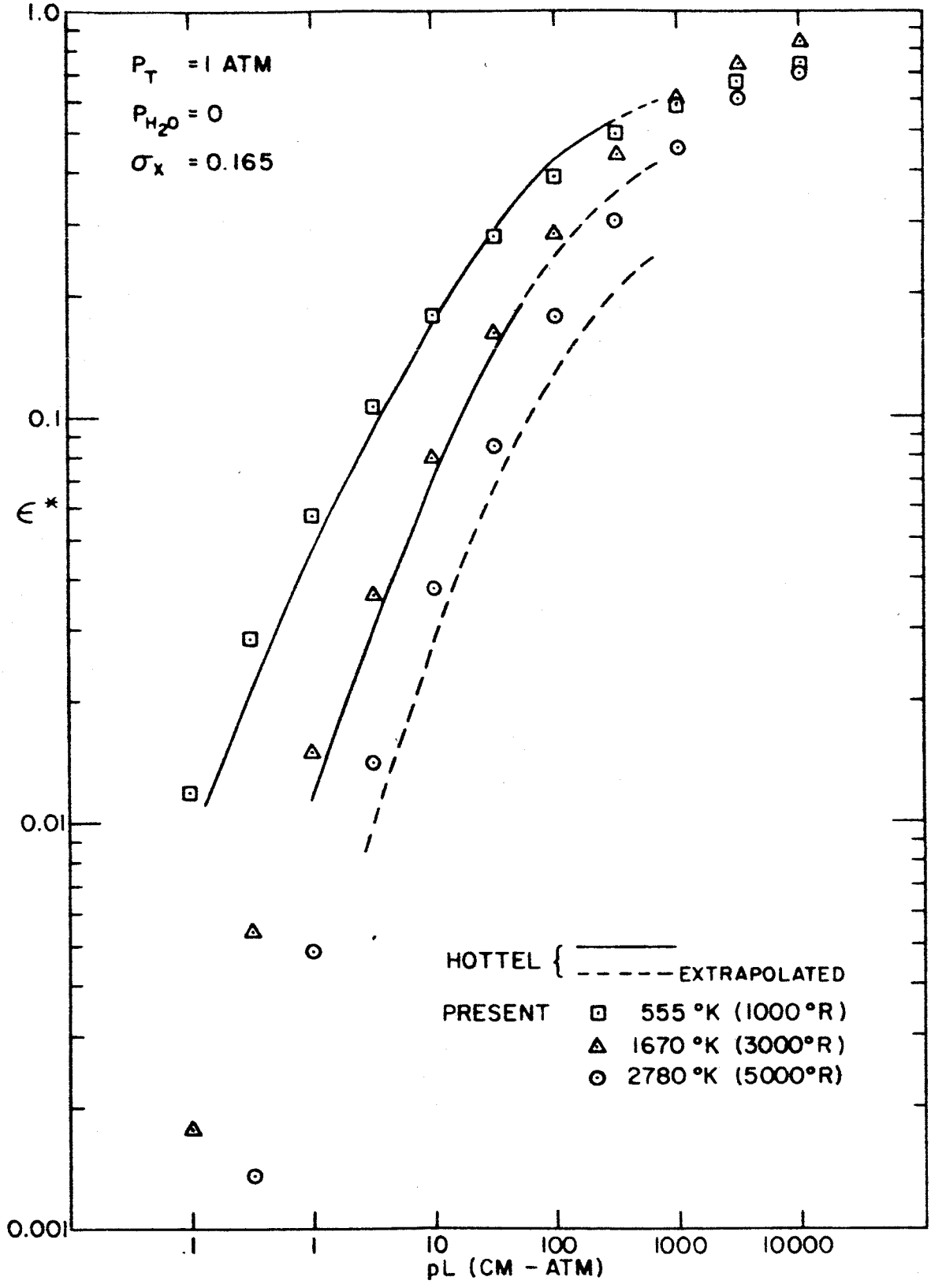

Fig. 28. Comparison of computed total emissivity of purely nitrogen-broadened water vapor with Hottel's[6] result at 555°, 1670°, and 2780°K at a total pressure of 1 atm.

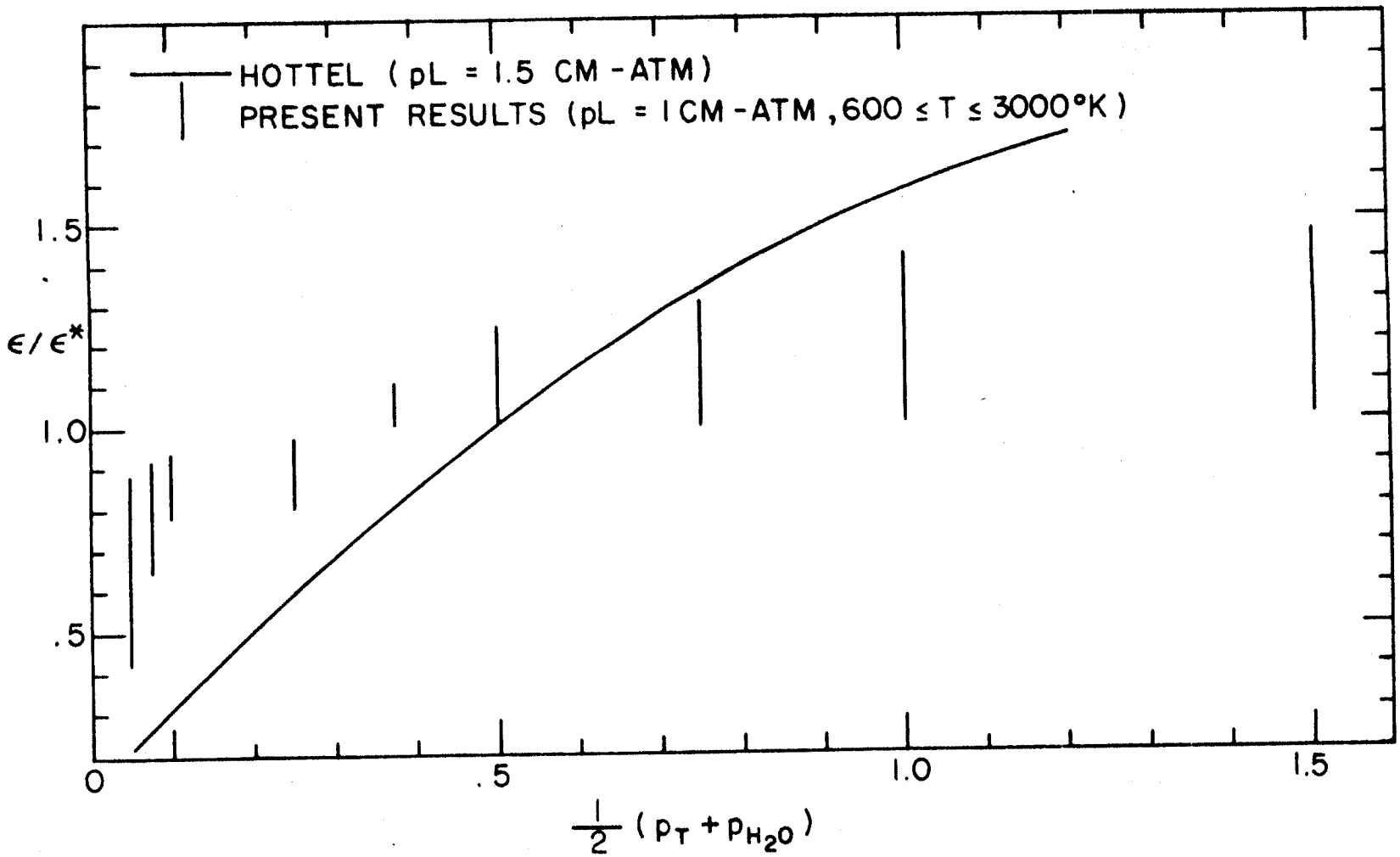

Fig. 29. Comparison of the ratio ϵ/ϵ^* between Hottel's and our results for pL ~ 1 cm atm.

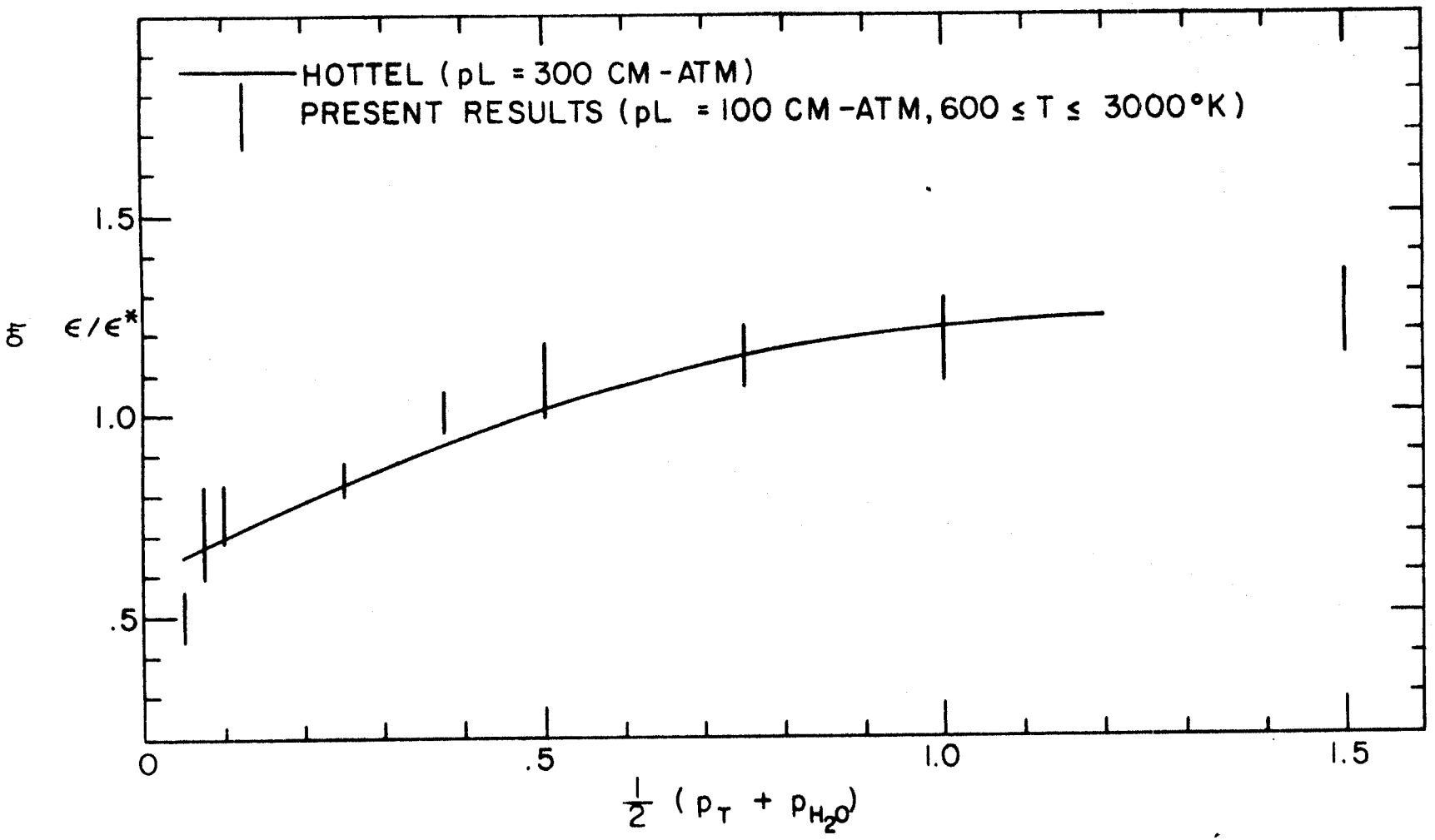

Fig. 30. Comparison of the ratio ϵ/ϵ^* between Hottel's and our results for pL ~ 100 cm atm.

TABLE I

COMPARISON OF MEASURED AND CALCULATED BAND ABSORPTION

T DEGR.K	W G/SQ M	PT ATM	C	A-EX 1/CM	A-CAL 1/CM	DEV PERCENT
ROTATION BAND (500-1000 1/CM)						
555.	306.6	2.	1.	292.	132.2	55
555.	153.3	1.00	1.0	202.	94.1	53
555.	90.9	.604	1.	102.	67.3	34
555.	16.3	2.75	.04	33.2	25.5	23
555.	16.3	.274	.40	22.6	17.2	24
555.	16.1	1.09	.10	26.5	21.4	19
555.	6.89	1.16	.04	13.9	11.6	17
555.	1.76	1.19	.01	9.5	3.8	60
833.	204.4	2.	1.0	293.	296.6	-1
833.	102.2	1.00	1.0	214.	219.2	-2
833.	108.1	1.09	1.	153.	226.5	-48
833.	60.5	.606	1.0	152.	163.1	-7
833.	10.9	.276	.40	31.3	46.7	-49
833.	10.9	1.09	.10	47.	60.9	-30
833.	10.9	2.75	.04	54.	74.0	-37
833.	4.56	1.16	.04	29.3	35.0	-19
833.	1.18	1.20	.01	8.7	13.0	-49
1111.	153.3	2.00	1.0	374.	374.2	-0
1111.	76.7	1.00	1.0	280.	287.8	-3
1111.	47.3	.603	1.0	192.4	222.9	-16
1111.	8.19	.273	.40	39.5	66.8	-70
1111.	8.16	1.10	.10	55.9	89.3	-60
1111.	8.14	2.75	.04	86.5	108.3	-25
1111.	3.45	1.16	.04	42.8	52.9	-23
1111.	.889	1.19	.01	14.1	20.1	-43
500.	2.60	1.0	.20	10.8	4.4	59
540.	2.57	1.0	.21	9.3	5.1	45
850.	2.39	1.0	.3	17.3	24.4	-41
620.	2.52	1.0	.23	9.6	7.9	17
1040.	2.31	1.0	.36	28.7	36.8	-28
1640.	2.26	1.0	.55	76.1	88.3	-16
1830.	2.28	1.0	.62	126.1	105.6	16
2200.	2.33	1.0	.74	149.4	136.7	8
2200.	2.33	1.0	.74	145.8	136.7	6
2750.	1.02	1.20	.648	78.8	93.4	-18
2750.	1.02	1.20	.648	82.8	93.4	-13
						(33 RMS)
6.3-MICRON BAND						
300.	14900.	0.016	1.	564.	643.4	-14
300.	12000.	.969	.014	745.	883.5	-19
300.	12000.	0.013	1.	545.	593.4	-9
300.	6870.	.969	.014	719.	811.4	-13
300.	6870.	.410	.032	659.	728.7	-11
300.	6870.	.083	.159	560.	599.3	-7

TABLE I (CONT.D)

T DEGR.K	W G/SQ M	PT ATM	C	A-EX 1/CM	A-CAL 1/CM	DEV PERCENT
300.	6870.	0.013	1.	477.	527.3	-11
300.	1720.	0.969	0.014	596.	637.7	-7
300.	1720.	0.382	0.0172	513.	545.5	-6
300.	1720.	0.007	1.	270.	301.4	-12
300.	1700.	0.003	1.	238.	221.4	7
300.	213.	0.162	0.0203	247.	230.2	7
300.	213.	0.072	0.0455	184.	177.0	4
300.	213.	0.013	0.25	130.	112.9	13
300.	213.	0.003	1.	66.	91.9	-39
300.	95.	0.945	0.0247	335.	303.0	10
300.	95.	0.526	0.0625	287.	268.2	7
300.	95.	0.263	0.125	236.	230.5	2
300.	95.	0.034	0.962	223.	176.3	21
300.	36.	1.00	0.004	216.	205.7	5
300.	34.	0.004	1.0	31.8	44.1	-39
300.	17.	0.101	0.0366	60.3	63.6	-6
300.	17.	0.004	1.0	25.0	31.3	-25
555.	307.	2.0	1.0	764.	814.4	-7
555.	153.	1.0	1.0	621.	650.5	-5
555.	89.	0.604	1.00	503.	502.8	0
555.	16.3	2.746	0.04	235.	244.6	-4
555.	16.3	1.091	0.10	178.7	200.1	-12
555.	16.3	0.274	.04	147.2	113.2	23
555.	15.3	1.094	0.10	182.	193.7	-6
555.	6.92	1.157	0.04	108.9	118.7	-9
555.	1.79	1.189	0.01	53.	46.2	13
833.	204.	2.00	1.0	766.	874.8	-14
833.	108.	1.09	1.0	542.	678.2	-25
833.	102.	1.00	1.0	594.	655.6	-10
833.	60.8	.606	1.0	479.	486.0	-1
833.	10.9	2.75	.04	194.7	214.3	-10
833.	10.9	1.09	.10	174.5	177.1	-1
833.	10.9	.276	.4	112.9	135.3	-20
833.	4.56	1.16	.04	106.3	99.4	6
833.	1.19	1.20	0.01	26.8	35.5	-32
1111.	153.	2.00	1.0	779.	903.6	-16
1111.	76.7	1.00	1.0	654.	655.1	-0
1111.	45.3	0.60	1.0	467.	470.4	-1
1111.	45.0	0.60	1.0	479.	469.0	2
1111.	8.23	2.75	0.04	193.2	195.6	-1
1111.	8.21	1.10	.1	153.2	165.1	-8
1111.	8.18	.273	.4	98.5	125.8	-28
1111.	3.49	1.16	.04	95.2	89.9	6
1111.	.887	1.19	.01	34.6	29.2	16
860.	2.39	1.0	.3	45.3	65.0	-43
1070.	2.3	1.0	.36	48.1	67.2	-39
1080.	2.3	1.0	.37	55.6	67.6	-21
1100.	2.3	1.0	.37	56.7	67.9	-20

TABLE I (CONT.D)

T DEGR.K	W G/SQ M	PT ATM	C	A-EX 1/CM	A-CAL 1/CM	DEV PERCENT
1140.	2.29	1.0	.38	61.1	68.5	-12
1300.	2.25	1.0	.43	81.2	70.8	13
1380.	2.25	1.0	.46	71.6	72.3	-1
1450.	2.25	1.0	.48	98.8	73.5	25
1450.	2.25	1.0	.48	95.1	73.5	22
1520.	2.25	1.0	.5	86.8	74.9	14
1520.	2.25	1.	.48	90.3	74.9	17
1535.	2.26	1.0	.55	80.7	76.0	6
1850.	2.28	1.0	.62	94.1	83.6	11
1930.	2.3	1.0	.65	97.0	86.0	11
2200.	2.33	1.0	.74	100.3	91.8	8
2200.	2.33	1.0	.74	100.0	91.8	8
2750.	1.02	1.2	.648	40.4	41.1	-2
2750.	2.04	1.2	.648	83.8	78.8	6
2750.	1.02	1.2	.648	43.2	46.4	-7
2750.	1.02	1.2	.648	45.3	46.4	-2
2750.	1.02	1.2	.648	44.1	46.4	-5
						(15 RMS)
	2.7-MICRON BAND					
300.	21000.	.397	0.054	1104.	1006.3	9
300.	21000.	0.171	0.125	1002.	900.4	10
300.	21000.	0.082	0.263	940.	837.0	11
300.	16800.	0.966	0.022	1158.	1101.5	5
300.	11200.	0.966	0.022	1064.	1018.7	4
300.	11200.	0.397	0.054	966.	888.0	8
300.	11200.	0.021	1.0	781.	672.8	14
300.	6440.	0.973	0.007	931.	898.9	3
300.	6440.	0.184	0.036	721.	661.9	8
300.	6440.	0.007	1.0	486.8	436.7	10
300.	2800.	0.966	0.022	809.	757.4	6
300.	2800.	0.397	.054	723.	655.5	9
300.	2800.	0.021	1.0	562.3	470.7	16
300.	1400.	0.966	0.022	699.	640.6	8
300.	1400.	0.397	0.054	623.2	549.3	12
300.	1400.	0.083	0.259	507.1	428.0	16
300.	644.	0.066	0.15	339.8	276.2	19
300.	644.	0.010	1.0	259.6	217.9	16
300.	172.	0.033	0.08	141.8	108.1	24
300.	172.	0.003	0.953	83.5	70.6	16
300.	23.8	1.00	0.008	155.	143.0	8
300.	23.8	.525	.015	125.	115.6	7
300.	23.8	0.066	0.12	59.	59.6	-1
300.	1010.	775.	0.028	664.	796.9	-20
300.	1010.	305.	0.072	582.	796.3	-37
300.	1010.	122.	0.178	518.	795.4	-54
300.	1010.	45.	0.469	462.	794.3	-72
555.	307.	2.0	1.0	740.	775.1	-5

TABLE I (CONT.D)

T DEGR.K	W G/SQ M	PT ATM	C	A-EX 1/CM	A-CAL 1/CM	DEV PERCENT
555.	153.	1.0	1.0	559.	602.2	-8
555.	89.	0.604	1.	470.7	456.1	3
555.	16.3	2.75	0.04	197.4	210.4	-7
555.	16.3	1.09	.10	156.	172.1	-10
555.	16.3	0.274	.40	116.3	132.8	-14
555.	15.3	1.09	0.10	151.2	166.2	-10
555.	6.92	1.16	0.04	96.4	99.9	-4
555.	1.78	1.19	0.01	32.6	36.8	-13
833.	204.	2.0	1.0	741.	805.8	-9
833.	108.	1.09	1.0	500.	613.0	-23
833.	102.	1.0	1.0	576.	591.3	-3
833.	60.8	0.606	1.0	425.	430.5	-1
833.	10.9	2.75	0.04	159.6	179.7	-13
833.	10.9	1.09	0.10	140.4	149.5	-6
833.	10.9	0.276	.40	99.4	114.8	-16
833.	4.56	1.16	0.04	81.3	81.6	-0
833.	1.19	1.20	0.01	24.5	27.6	-13
1111.	153.	2.0	1.0	785.	837.4	-7
1111.	76.7	1.0	1.0	560.	585.4	-5
1111.	45.3	0.603	1.0	406.	410.3	-1
1111.	45.0	0.603	1.0	416.	409.0	2
1111.	8.23	2.750	0.04	135.	156.4	-16
1111.	8.21	1.10	.10	126.	134.3	-7
1111.	8.18	0.273	0.40	101.	104.1	-3
1111.	3.49	1.16	0.04	77.	70.4	9
1111.	0.887	1.19	0.01	22.	21.5	2
900.	1.19	.0625	1.	13.9	20.9	-50
900.	2.41	.127	1.	45.4	41.7	8
900.	4.71	.249	1.	77.5	79.4	-2
900.	9.45	.5	1.	156.0	150.1	3
900.	18.8	1.	1.	291.	270.6	7
1200.	3.55	.249	1.	80.	67.4	15
1200.	7.1	.5	1.	146.	129.6	11
1200.	14.1	1.	1.	248.	238.7	4
1500.	1.44	.127	1.	26.9	29.9	-11
1500.	2.84	.249	1.	49.4	57.9	-17
1500.	5.69	.5	1.	135.0	112.7	16
545.	2.57	1.	.21	56.1	49.8	11
980.	2.33	1.	.34	43.7	50.8	-16
1220.	2.27	1.	.4	47.9	50.8	-6
1500.	2.24	1.	.5	51.8	51.2	1
1830.	2.28	1.	.61	54.	54.3	-1
2150.	2.32	1.	.72	69.5	58.3	16
2750.	1.03	1.2	.648	28.3	28.7	-1
2750.	.96	1.12	.645	26.3	26.8	-2
2750.	1.92	1.12	.645	54.9	52.6	4
2750.	1.02	1.2	.648	28.2	28.4	-1
						(16 RMS)

TABLE I (CONT.D)

T DEGR.K	W G/SQ M	PT ATM	C	A-EX 1/CM	A-CAL 1/CM	DEV PERCENT
	1.87-MICRON BAND					
300.	38500.	0.132	0.280	572.	479.5	16
300.	18500.	0.141	0.092	458.	390.8	15
300.	14300.	0.013	1.0	345.	289.3	16
300.	5310.	0.368	.019	407.	337.4	17
300.	5310.	0.026	0.26	216.	187.3	13
300.	5310.	0.007	1.0	182.	164.8	9
300.	1710.	0.973	0.89	395.	416.8	-6
300.	1710.	0.263	0.195	314.	261.8	17
300.	1710.	0.058	0.053	271.	127.4	53
300.	480.	0.973	0.022	229.	207.8	9
300.	480.	0.507	0.015	207.	164.6	20
300.	480.	0.022	0.941	114.	93.6	18
300.	120.	0.973	0.022	126.	113.2	10
300.	120.	0.0224	.941	51.	49.1	4
300.	33.	1.0	0.007	51.1	54.5	-7
300.	33.	0.405	0.018	38.0	41.0	-8
300.	33.	0.161	0.045	27.0	29.9	-11
300.	33.	0.061	0.12	19.3	22.2	-15
300.	33.	0.0072	1.0	11.7	15.6	-33
555.	307.	2.00	1.00	291.	358.3	-23
555.	153.	1.00	1.00	164.	226.0	-38
555.	89.	0.604	1.0	124.	147.9	-19
555.	16.3	2.75	0.04	41.	42.9	-5
555.	16.3	1.09	0.10	33.7	38.9	-15
555.	16.3	0.274	0.40	36.1	33.2	8
555.	15.3	1.09	0.10	30.0	37.0	-23
555.	6.92	1.16	0.04	19.0	18.7	2
833.	204.	2.0	1.0	244.	359.7	-47
833.	108.	1.09	1.0	132.	220.9	-67
833.	102.	1.0	1.0	157.	209.5	-33
833.	60.8	0.606	1.0	121.	133.9	-11
833.	10.9	2.75	0.04	28.1	33.3	-19
833.	10.9	1.09	0.10	27.6	31.4	-14
833.	10.9	.276	0.40	32.3	27.9	14
1111.	153.	2.00	1.0	260.	360.4	-39
1111.	76.7	1.0	1.0	152.	203.3	-34
1111.	45.3	0.603	1.0	106.	126.8	-20
1111.	45.0	0.603	1.0	107.	126.2	-18
1111.	8.23	2.75	0.04	27.	29.6	-9
1111.	8.21	1.10	0.10	28.3	28.3	-0
1111.	8.18	0.273	0.40	24.9	25.7	-3
1111.	3.49	1.16	0.04	22.6	12.7	44
880.	2.37	1.0	.31	9.3	7.7	17
1020.	2.32	1.0	.34	8.	7.9	1
1100.	2.3	1.0	.37	9.3	8.4	10
1160.	2.28	1.0	.39	8.1	8.6	-7
1200.	2.27	1.0	.4	7.8	8.8	-13

TABLE I (CONT.D)

T DEGR.K	W G/SQ M	PT ATM	C	A-EX 1/CM	A-CAL 1/CM	DEV PERCENT
1550.	2.25	1.0	.51	10.6	10.6	0
1580.	2.25	1.	.53	10.3	10.7	-3
1600.	2.25	1.0	.53	11.7	10.7	8
1620.	2.26	1.	.54	11.1	10.8	2
1650.	2.26	1.0	.55	10.6	10.9	-2
1680.	2.26	1.0	.56	11.6	11.0	5
1750.	2.27	1.	.59	11.6	11.3	3
1900.	2.29	1.0	.64	12.6	11.9	6
1900.	2.3	1.0	.64	11.8	11.9	-1
2150.	2.32	1.	.72	13.7	13.1	4
2150.	2.32	1.	.72	12.7	12.6	1
2250.	2.34	1.0	.75	18.1	13.1	27
2250.	2.34	1.0	.75	20.8	13.1	37
2250.	2.34	1.0	.75	14.0	13.1	6
						(21 RMS)
1.38-MICRON BAND						
300.	5310.	0.0263	0.26	282.	199.0	29
300.	5310.	0.0068	1.0	257.	170.5	34
300.	4120.	0.0039	1.0	147.	120.1	18
300.	4120.	0.263	0.015	348.	317.8	9
300.	2400.	0.131	0.28	338.	274.0	19
300.	2400.	0.037	1.0	303.	242.7	20
300.	880.	0.973	0.007	334.	272.0	19
300.	880.	0.368	0.0185	238.	197.4	17
300.	880.	0.0696	0.98	147.	203.2	-38
300.	880.	0.0068	1.0	99.	76.2	23
300.	440.	0.973	.007	311.	201.4	35
300.	440.	0.166	0.0412	143.	109.3	24
300.	440.	0.0068	1.00	73.	54.8	25
555.	307.	2.00	1.00	303.	345.9	-14
555.	153.	1.00	1.00	194.	209.1	-8
555.	89.	0.604	1.00	121.	134.1	-11
555.	16.3	2.75	0.04	29.4	36.3	-23
555.	16.3	0.274	0.40	31.7	29.1	8
555.	15.3	1.09	0.10	33.7	31.7	6
833.	204.	2.00	1.00	239.	313.2	-31
833.	108.	1.09	1.00	101.	187.9	-86
833.	102.	1.00	1.00	144.	178.0	-24
833.	60.8	0.606	1.00	113.	112.5	0
833.	10.9	1.09	0.10	27.7	25.3	9
1111.	153.	2.00	1.00	217.	286.4	-32
1111.	76.7	1.00	1.00	124.	157.6	-27
1111.	45.3	0.603	1.00	76.0	97.2	-28
1111.	45.0	0.603	1.00	79.5	96.7	-22
1111.	8.2	1.10	0.1	22.7	20.8	9
1020.	2.32	1.0	.34	7.7	6.1	21
1020.	2.32	1.0	.35	6.0	6.0	0

TABLE I (CONT.D)

T DEGR.K	W G/SQ M	PT ATM	C	A-EX 1/CM	A-CAL 1/CM	DEV PERCENT
1160.	2.28	1.0	.39	5.0	6.1	-23
1240.	2.26	1.0	.41	6.1	6.2	-2
1400.	2.25	1.0	.46	6.4	6.5	-1
1540.	2.25	1.0	.51	8.3	6.7	19
1550.	2.25	1.0	.51	7.5	6.8	10
1580.	2.25	1.	.53	7.6	6.9	9
1600.	2.25	1.0	.53	7.9	7.0	12
1620.	2.25	1.0	.54	6.6	7.0	-6
1620.	2.26	1.	.54	8.0	7.0	12
1650.	2.26	1.0	.55	7.1	7.1	-1
1680.	2.26	1.0	.56	6.9	7.3	-5
1750.	2.27	1.	.59	8.2	7.6	8
1830.	2.28	1.0	.61	8.1	7.9	3
1900.	2.29	1.0	.64	8.9	8.2	8
1900.	2.3	1.0	.64	7.7	8.2	-6
1950.	2.3	1.0	.65	8.2	8.4	-2
1960.	2.3	1.0	.65	8.3	8.4	-1
2150.	2.32	1.	.72	8.6	8.9	-3
2150.	2.32	1.	.72	8.2	8.9	-7
2250.	2.34	1.0	.75	11.7	9.1	22
2250.	2.34	1.0	.75	10.6	9.1	14
2250.	2.34	1.0	.75	9.7	9.1	6
2250.	2.34	1.0	.75	9.8	9.1	7
						(21 RMS)